HIPPOCAMPUS 00:00–00 (2014)

The Hippocampal CA3 Region Can Generate Two Distinct Types of Sharp Wave-Ripple Complexes, In Vitro

Katharina T. Hofer,[1,2] Ágnes Kandrács,[1,2] István Ulbert,[1,2,3] Ildikó Pál,[1] Csilla Szabó,[1,2] László Héja,[1] and Lucia Wittner[1,3]*

AQ1 **ABSTRACT: Hippocampal sharp wave-ripples (SPW-Rs) occur during slow wave sleep and behavioral immobility and are thought to play an important role in memory formation. We investigated the cellular and network properties of SPW-Rs with simultaneous laminar multielectrode and intracellular recordings in a rat hippocampal slice model, using physiological bathing medium. Spontaneous SPW-Rs were generated in the dentate gyrus (DG), CA3, and CA1 regions. These events were characterized by a local field potential gradient (LFPg) transient, increased fast oscillatory activity and increased multiple unit activity (MUA). Two types of SPW-Rs were distinguished in the CA3 region based on their different LFPg and current source density (CSD) pattern. Type 1 (T1) displayed negative LFPg transient in the pyramidal cell layer, and the associated CSD sink was confined to the proximal dendrites. Type 2 (T2) SPW-Rs were characterized by positive LFPg transient in the cell layer, and showed CSD sinks involving both the apical and basal dendrites. In both types, consistent with the somatic CSD source, only a small subset of CA3 pyramidal cells fired, most pyramidal cells were hyperpolarized, while most interneurons increased firing rate before the LFPg peak. Different neuronal populations, with different proportions of pyramidal cells and distinct subsets of interneurons were activated during T1 and T2 SPW-Rs. Activation of specific inhibitory cell subsets—with the possible leading role of perisomatic interneurons—seems to be crucial to synchronize distinct ensembles of CA3 pyramidal cells finally resulting in the expression of different SPW-R activities. This suggests that the hippocampus can generate dynamic changes in its activity stemming from the same excitatory and inhibitory circuits, and so, might provide the cellular and network basis for an input-specific and activity-dependent information transmission.** © 2014 Wiley Periodicals, Inc.

KEY WORDS: rat; linear multielectrode; network oscillation; perisomatic interneuron; current source density

[1] **Institute of Cognitive Neuroscience and Psychology, Research Center for Natural Sciences, Hungarian Academy of Sciences, Budapest, Hungary;** [2] **Department of Information Technology, Péter Pázmány Catholic University, Budapest, Hungary;** [3] **National Institute of Clinical Neuro-**
AQ3 **sciences, Budapest, Hungary.**

Additional Supporting Information may be found in the online version of this article.

Grant sponsor: Bolyai János Research Fellowship; Grant numbers: OTKA PD77864; OMFB-0166/2009; Grant sponsor: ERA-Chemistry; Grant numbers: OTKA 102166; KMR_12-1-2012-0112 TRANSRAT; Grant sponsor: NKTH-ANR Neurogen, NKTH-ANR Multisca; Grant number: OTKA K81357; Grant sponsor: TÁMOP; Grant number: 4.2.1.B-11/2/KMR-2011-0002; Grant sponsor: Pázmány Péter Catholic University.

Abbreviations used: AMPA, α-amino-3-hydroxyl-5-methyl-4-isoxazole-propionate; CA, cornu Ammonis; CB1, cannabinoid receptor, type 1; CCh, carbachol; CSD, current source density; DG, dentate gyrus; GABA, γ-amino-butyric acid; h, hilus; KA, kainite; LFPg, local field potential gradient; MF, mossy fiber; mGluR2, type II metabotropic glutamate receptor; MUA, multiple unit activity; NMDA, *N*-methyl-D-aspartate; PETH, peri-event time histogram; PV, parvalbumin; RMP, resting membrane potential; SD, standard deviation; SEM, standard error of the mean; SPW-R, sharp wave-ripple; str. gr, stratum granulosum (granule cell layer); str. lac-mol, stratum lacunosum-moleculare; str. mol, stratum molecular; str. ori, stratum oriens; str. pyr, stratum pyramidale (pyramidal cell layer); str. rad, stratum radiatum; T1, Type 1; T2, Type 2; TFR, time-frequency plot.

*Correspondence to: Lucia Wittner, Institute of Cognitive Neuroscience and Psychology, Research Center for Natural Sciences, Hungarian Academy of Sciences, 1117 Budapest, Magyar Tudósok körútja 2, Hungary.
E-mail: wittner.lucia@ttk.mta.hu

Accepted for publication 5 September 2014.
DOI 10.1002/hipo.22361
Published online 00 Month 2014 in Wiley Online Library (wileyonlinelibrary.com).

INTRODUCTION

Sharp wave-ripple complexes have been observed in the hippocampus of rodents during slow wave sleep and behavioral immobility (Buzsáki et al., 1983). These synchronous population bursts are thought to have an important role in memory consolidation within the hippocampus and in conversion into long-term memory trace (Buzsáki, 1989). Hippocampal SPW-Rs have been associated with large field potential deflections and high frequency oscillatory ripple activity (Buzsáki et al., 1992; Ylinen et al., 1995). The generation of SPW-Rs is thought to depend on synchronous firing in a small subset of CA3 pyramidal cells together with an enhanced discharge rate of interneurons (Csicsvári et al., 2000).

In vitro models of SPW-Rs activity also consist of rhythmically recurring field potential transients accompanied by high frequency oscillations and increased neuronal firing, showing striking similarities with SPW-Rs occurring in vivo. In vitro population events are typically initiated in the hippocampal CA3 region, and spread to the DG, CA1 region and subiculum (Papatheodoropoulos and Kostopoulos, 2002a; Kubota et al., 2003; Maier et al., 2003; Kano et al., 2005; Nimmrich et al., 2005; Wu et al., 2006). Different neural responses of CA3 pyramidal cells have been described during SPW-Rs in vitro. In some

J_ID: za4 Customer A_ID: HIPO22361 Cadmus Art: HIPO22361 Ed. Ref. No.: 13-341.R2 Date: 16-September-14 Stage: Page: 2

models, hyperpolarizing, depolarizing or mixed responses were detected (Behrens et al., 2005; Wu et al., 2005b; Ellender et al., 2010), while in other studies pyramidal cells either fired or received only excitatory synaptic currents during SPW-Rs (Colgin et al., 2004a; Wu et al., 2005a).

The role of inhibitory cells in the generation of SPW-Rs in vitro seems to be crucial (Ellender et al., 2010; Hájos et al., 2013). Hippocampal interneurons may be classified into different functional groups. Perisomatic interneurons (parvalbumin, PV-positive axo-axonic and basket cells and type 1 cannabinoid receptor, CB1-positive basket cells) innervate the axon initial segments and the somatic region of principal cells, controlling their output, while dendritic inhibitory cells project their axons to the dendritic region of principal cells to influence their inputs. The interneuron-selective interneurons specifically innervate inhibitory cells and are supposed to have a role in network synchronizations (Freund and Buzsáki, 1996; Miles et al., 1996; Freund and Katona, 2007). GABAergic signaling is generally agreed to regulate the generation of SPW-Rs in vitro (Papatheodoropoulos and Kostopoulos, 2002a; Maier et al., 2003; Nimmrich et al., 2005). A recent study examined the firing behavior during SPW-Rs of different interneuron types in mouse hippocampal slices (Hájos et al., 2013). Parvalbumin-containing basket cells were found to be the most active during SPW-Rs, whereas axo-axonic cells and CB1-positive basket interneurons were recruited to a lesser extent.

In this study, we aimed to reveal the cellular and network properties of spontaneously occurring SPW-Rs in rat hippocampal slices. The use of laminar multielectrodes let us perform detailed LFPg, MUA and CSD analyses of their spatio-temporal properties. We found that DG, CA3, and CA1 can generate spontaneous SPW-Rs in vitro. In the CA3 region, two types of SPW-Rs exhibited differences in recurrence frequency, LFPg pattern and amplitude, MUA increase and CSD pattern. Simultaneous intra- and extracellular recordings of CA3 pyramidal cells and interneurons, as well as pharmacological manipulations indicated that distinct interneuron populations (with the leading role of perisomatic interneurons) are activated during the different SPW-Rs and recruit different ensembles of CA3 pyramidal cells.

MATERIALS AND METHODS

Slice Preparation

All experiments were performed according to the EC Council Directive of November 24, 1986 (86/89/EEC) and all procedures were reviewed and approved by the local ethical committee and the Hungarian Central Agricultural Office (license number: 22.1/4228/003/2009). Hippocampal slices were prepared from adult Wistar rats of weight 200–500 g (postnatal Days 28–180), from both sexes. Animals were anaesthetized intraperitoneally with urethane (1,000 mg/kg) and perfused intracardially with a solution of 248 mM sucrose, 26 mM $NaHCO_3$, 1 mM KCl, 10 mM $MgCl_2$, 1 mM $CaCl_2$, and 10 mM glucose, equilibrated with 5% CO_2−95% O_2 at 3–5°C. After perfusion, animals were decapitated, both hemispheres dissected, and horizontal slices of 500 μm thickness were prepared from the ventral hippocampus and adjacent neocortical areas. In a set of experiments, we isolated the dentate gyrus, the CA3 and CA1 regions by cutting intrahippocampal connections immediately after the cutting procedure. One cut was made at the border between CA3 and CA1 regions, and another at the end of the two blades of the dentate gyrus. Slices were then transferred to an interface recording chamber at 34–35°C, and perfused with a physiological solution containing 124 mM NaCl, 26 mM $NaHCO_3$, 4 mM KCl, 2 mM $MgCl_2$, 2 mM $CaCl_2$, and 10 mM glucose, equilibrated with 5% CO_2−95% O_2. Slices recovered in our standard ACSF solution for at least 1 h before starting electrophysiological recording. In a subset of experiments (comparing gradient and referential recordings) slices recovered for at least 1 h, and were then stored in a separate interface chamber (in our standard ACSF, at 35°C) before they were transferred to a dual perfusion submerged chamber, also kept at 35°C and perfused with the physiological solution described above.

Drugs

A type γ-aminobutyric acid ($GABA_A$) receptor mediated signaling was suppressed by bicuculline methiodide (10 μM). $GABA_B$ receptors were blocked by 3-[[(3,4-Dichlorophenyl)-methyl]amino]propyl] diethoxymethyl)phosphinic acid CGP52432 (2 μM). AMPA (α-amino-3-hydroxyl-5-methyl-4-isoxazole-propionate) and KA (kainate) type glutamate receptors were blocked using 2,3-dihydroxy-6-nitro-7-sulfamoyl-benzo(f)quinoxaline (5 μM, NBQX) and NMDA (*N*-methyl-D-aspartate) type receptors were blocked with D,L-2-amino-5-phosphonovaleric acid (50 μM, D,L-APV). The mu opioid receptor agonist DAMGO ([D-Ala 2,N-Me-Phe4,Gly 5-ol]enkephalin acetate, 1 μM) and the acetylcholine receptor agonist carbachol (CCh, 5 μM) was used to reduce the activity of parvalbumin-positive basket and somatostatin-positive O-LM cells (Freund and Buzsáki, 1996; Drake and Milner, 2002; Gulyás et al., 2010) and cholecystokinin (CCK)/Type 1 cannabinoid receptor (CB1)-positive (Szabó et al., 2010) basket cells, respectively. The Type II metabotropic glutamate receptor (mGluR2) agonist DCG-IV ((2*S*,2′*R*,3′*R*)-2-(2′,3′-Dicarboxycyclopropyl)glycine) was used to block the activity of mossy fibers (1 μM, (Kamiya et al., 1996). Drugs were obtained from Tocris Bioscience (Izinta Kft., Hungary), except CCh, which was purchased from Sigma-Aldrich.

Recordings

Intracellular records were made with microelectrode pipettes that contained 2 M K-Acetate beveled to a resistance of 50–100 MΩ. The data were obtained within 10–20 min of cell penetration. Signals were amplified with a BA-1S (NPI Electronic GmbH, Tamm, Germany) amplifier operated in current-clamp mode. In acceptable neuronal records,

ID: parasuramank Time: 14:11 I Path: N:/3b2/HIPO/Vol00000/140122/APPFile/JW-HIPO140122

J_ID: za4 Customer A_ID: HIPO22361 Cadmus Art: HIPO22361 Ed. Ref. No.: 13-341.R2 Date: 16-September-14 Stage: Page: 3

membrane potential was more negative than −50 mV, input resistance was higher than 20 MΩ, and action potentials were overshooting.

The LFPg was recorded with laminar multielectrode array (24 channels, 50 μm intercontact distance) using a custom made voltage gradient amplifier of pass band 0.01 Hz–10 kHz (Ulbert et al., 2001; Ulbert et al., 2004a,b; Fabó et al., 2008). Signals were digitized with a 32 channel, 16 bit resolution analog-to-digital converter (National Instruments, Austin, TX) and recorded at 20 kHz sampling rate, using a home written routine in LabView7 (National Instruments, Austin, TX). The laminar multielectrode array was placed on the surface of the hippocampal slice, perpendicularly to the granule or pyramidal cell layer. In this way the whole extent of the examined region was covered by the microelectrode, so that extracellular recordings were made from each hippocampal layer.

In a subset of experiments gradient and referential recordings were simultaneously performed with two separate systems on slices kept in a dual perfusion chamber (Hájos et al., 2009). Referential recordings were made with extracellular glass electrodes (2–5 MΩ) filled with physiological ACSF solution. The glass electrode was placed in the pyramidal cell layer, 50–300 μm far from the linear multielectrode, whereas the reference electrode was in the bath solution. Signals coming from the glass electrode were recorded with a two-channel Multiclamp 700A amplifier (Axon Instruments, Foster City, CA). Traces were low-pass filtered at 2 kHz and digitized at 10 kHz with a Digidata 1320A A/D board (Axon Instruments, Foster City, CA) controlled by a computer running pClamp8 (Axon Instruments, Foster City, CA). Gradient recordings were simultaneously and separately performed with the linear multielectrode, as described above.

Stimulation was made with a tungsten bipolar electrode made from two 1 MΩ impedance, 100 μm diameter FHC electrodes (FHC Inc. Bowdoin, ME), with a tip distance of about 80–100 μm, placed either in the granule cell layer of the dentate gyrus (to stimulate mossy fibers) or at the border of the str. pyramidale and oriens of the CA3a region (to stimulate CA3 recurrent collaterals). We tried to be very careful to avoid the stimulation of other pathways then the desired one. We recorded spontaneous SPW-Rs and the activation pattern of mossy fiber or CA3 recurrent collaterals in the CA3b region. BioStim stimulator system (Supertech Pécs, Hungary) was used, with settings of 0.2 ms stimulus length, 1,000 ms interstimulus interval and 0.02–0.05 mA stimulus intensity.

We examined the effects of drugs applied as follows. The dropping speed of our gravity operated bathing system was set to 4–6 ml/min. The development of drug action was related to the amount of bathing solution flowed through the recording chamber. The ACSF volume needed to fill the tubing system and the recording chamber is about 20 ml. In all pharmacological experiments we used a quantity of 100 ml of ACSF containing the drug to be tested. Before drug application we checked the presence of SPW-Rs in all slices of the first recording chamber. We chose a slice generating SPW-Rs and recorded for at least 20 min in control conditions to check the stability of the population activity. If the SPW-R activity was stable (which was usually the case), the last 3 min before placing the tube to the bath containing the drug was used as control segment. The effect of the drug started to be visible after 5–8 min (∼30 ml of ACSF + drug), and became stable after about 10 min (∼40 ml of ACSF + drug). The last 3 min before changing back to the control ACSF solution (about 10 min after the development of the stable drug effect) was analyzed as drug effect. As washout segment, we analyzed a 3 min recording after about 30 min perfusing the chamber with control ACSF in the case of all drugs except bicuculline, which took about 1.5–2 h to be washed out.

Data Analysis

Data were analyzed with the Neuroscan Edit 4.5 program (Compumedics Neuroscan, Charlotte, NC) and routines written for Matlab (The MathWorks, Natick, MA). Current source density, which estimates population trans-membrane currents, and multiple unit activity were calculated from the LFPg using standard techniques (Ulbert et al., 2004a,b; Fabó et al., 2008). Briefly, the CSD was obtained from LFPg records by applying one additional spatial derivation, after a Hamming-window spatial smoothing. A continuous estimate of MUA was obtained by high pass filtering (500 Hz, zero phase shift, 48 dB/octave), and full wave rectification of original records.

Sharp waves were detected from LFPg recordings, after applying 2× Hamming window spatial smoothing and bandpass filtering between 1 and 30 Hz, using an amplitude threshold of 3× standard deviation (SD), with routines written in Matlab. The peak of the LFPg in the cell layer was used as time zero for further event triggered averaging. Baseline correction (−150 to −50 ms) was applied to averaged LFPg, CSD, and MUA (at least 50, but typically ∼100 to 350 events were averaged). In the color maps, CSD sinks are presented in red, sources in blue. Warm colors (red) depict MUA-increases and cold colors (blue) depict MUA decreases compared with baseline. Both the LFPg and MUA amplitudes of SPW-Rs were determined in the pyramidal cell layer, on the channel showing the largest amplitude. MUA integrals were calculated with the aid of a routine written for Matlab.

Ripple power and frequency were determined with the aid of routines written in Matlab, as follows. Wavelet analysis was applied on epochs (from −1,000 ms to 1,000 ms) with the LFPg peak of the SPW-R at time zero (detected as above). Time-frequency analysis was performed between 0 and 300 Hz on electrode channels located in the pyramidal cell layer, and baseline corrected to −300 to −100 ms. For each channel, both the exact values (μV^2 scale) and the maximal power change (relative to the baseline, dB scale) were determined within the range of 150–300 Hz, as well as the frequency where the power showed the maximum. Both the power and the frequency were averaged across channels, to receive one absolute (μV^2) and one relative (dB) power and one frequency parameter for each recording.

Peri-event time histograms (PETH) were derived from routines written in Matlab. To determine the interneuronal

ID: parasuramank Time: 14:11 I Path: N:/3b2/HIPO/Vol00000/140122/APPFile/JW-HIPO140122

J_ID: za4 Customer A_ID: HIPO22361 Cadmus Art: HIPO22361 Ed. Ref. No.: 13-341.R2 Date: 16-September-14 Stage: Page: 4

discharge pattern, the timing of neuronal firing, detected and clustered in high-pass filtered recordings (500 Hz, zero phase shift, 48 dB/octave), was compared to that of SPW-Rs. Spikes were clustered either with routines written in Matlab or with the program Klusters (Hazan et al., 2006). Only neurons with a clear refractory period of at least 1.5 ms were included. First, interneurons were identified by their location: cells detected outside of the pyramidal cell layer were considered as interneurons, and included in the analysis ($n = 47$ neurons). To identify interneurons of the pyramidal cell layer we examined the waveform of the averaged action potential (AP, derived from wide band recordings) and the autocorrelogram of the cell (Supporting Information Fig. 1, Csicsvári et al., 1999). If the AP width measured at the half amplitude was less than 0.25 ms, the cell was considered as interneuron, if it was larger than 0.5 ms, the cell was taken as pyramidal cell. If the AP width was between 0.25 and 0.5 ms, we examined the autocorrelogram. Cells with uncertain AP width and noncharacteristic autocorrelogram were excluded from the analysis. We did not observe cells with contradictory AP width and autocorrelogram. With this method we clustered 31 interneurons in the str. oriens, 24 interneurons, 17 pyramidal cells, and excluded 4 cells in the str. pyramidale, 13 interneurons in str. lucidum+radiatum, 2 interneurons in str. lacunosum-moleculare, 1 interneuron and 3 mossy cells in the hilus (a total of 71 interneurons). Peak firing was determined from PETH with 1 ms bins, and was compared to the peak of the LFPg average of the SPW-R.

Statistics

With the aid of the program SigmaStat3.0.1 (Systat software, San Jose, CA) a *t*-test or one-way ANOVA on ranks was used if data were normally distributed. Nonparametric Kruskall–Wallis ANOVA or Mann–Whitney rank sum test were used if the normality test was not satisfied.

RESULTS

Hippocampal SPW-Rs, In Vitro

Spontaneous synchronous population activity was generated in the ventral hippocampus of the rat, in vitro, in a physiological bathing solution. They were detected in the dentate gyrus (DG, $n = 26/82$ slices), and in the CA3 ($n = 147/274$ slices) and CA1 regions ($n = 6/34$ slices, Table 1). These population bursts were observed most frequently in the slices taken from between Bregma −7 and −5 in the dorso-ventral axis (Paxinos and Watson, 1998). LFPg was recorded with a 24-channel, 50 μm intercontact distance laminar multielectrode array placed perpendicular to the cell layer, to record from the entire somato-dendritic axis of the examined region. The synchronous population events consisted of increased high frequency LFPg oscillations and MUA superimposed on an LFPg transient. They were apparently similar to in vivo sharp wave ripple complexes (Buzsáki, 1986), and to synchronous population bursts previously recorded in rodent hippocampal slices, considered as in vitro models of SPW-Rs (Papatheodoropoulos and Kostopoulos, 2002a; Kubota et al., 2003; Maier et al., 2003; Colgin et al., 2004a; Behrens et al., 2005; Wu et al., 2005a,b; Foffani et al., 2007; Ellender et al., 2010). Therefore, these in vitro synchronous population events will be called SPW-Rs in the present study. We have to note that the synchronous population activity recorded previously in the DG was termed dentate wave in rat (Colgin et al., 2004b), SPW-R (Maier et al., 2003) or spontaneous rhythmic field potential (Wu et al., 2005b) in mouse hippocampal slices. CSD analysis, which estimates transmembrane currents in the local neuronal population (Freeman and Nicholson, 1975; Nicholson and Freeman, 1975), confirmed that SPW-Rs were locally generated in each of the DG, CA1, and CA3 regions in hippocampal slices with conserved intrahippocampal connections. CSD revealed differences between SPW-R events in the DG and those generated in the CA1 and CA3 regions. Current source density analysis showed a sink, corresponding to either an inward current representing active excitation or a passive return current, in the granule cell layer. In contrast, a source, corresponding to an outward, active inhibitory current or a passive return current, was found in stratum pyramidale of both CA1 and CA3 regions (Supporting Information Fig. 2).

It is a debated question whether the different subregions of the hippocampus can independently generate SPW-Rs in vitro, and what is the role of the intrahippocampal excitatory pathways (Maier et al., 2003; Colgin et al., 2004a; Wu et al., 2005a). We explored how SPW-R generation changes in our model in the different hippocampal regions when intrahippocampal connections are cut. Therefore, we recorded from mini slices containing either the DG, or the CA3 or the CA1 region, and found that SPW-Rs were generated in the CA3 region ($n = 9/16$ slices) and in the DG ($n = 2/9$ slices), but not in the CA1 region ($n = 0/9$ slices). We have to note that the DG mini slice contained the CA3c region between the two blades, and so, we cannot rule out the possibility that the observed population activity backpropagated from the CA3c region. In summary, we have observed that both the dentate gyrus and the CA3 region, but not the CA1 region can generate SPW-Rs independent of the other regions.

Different SPW-R Patterns in the CA3 Region

The CA3 region was suggested to serve as the generator region of SPW-Rs in vivo (Buzsáki, 1986; Csicsvári et al., 2000) and in vitro (Kubota et al., 2003; Maier et al., 2003; Colgin et al., 2004a; Behrens et al., 2005; Wu et al., 2005a,b; Foffani et al., 2007; Ellender et al., 2010). Accordingly, we concentrated our investigation on this region. SPW-Rs were recorded in all three subregions of the CA3 region (CA3a: $n = 20/83$ slices, CA3b: $n = 94/208$ slices, CA3c: $n = 33/103$ slices, total: $n = 147$ SPW-Rs/394 examined subregions in 274 slices).

ID: parasuramank Time: 14:11 I Path: N:/3b2/HIPO/Vol00000/140122/APPFile/JW-HIPO140122

J_ID: za4 Customer A_ID: HIPO22361 Cadmus Art: HIPO22361 Ed. Ref. No.: 13-341.R2 Date: 16-September-14 Stage: Page: 5

TABLE 1.

Number and Ratios of SPW-R Activities Detected in the Different Regions and Subregions of the Hippocampus

	Number of examined region or subregion	Number of activities recorded *n* (% of slices)	T1 SPW-Rs		T2 SPW-Rs		T1 + T2 SPW-Rs	
			n	% of slices % of activities	*n*	% of slices % of activities	*n*	% of slices % of activities
CA3a	83	20 (24.1%)	3	3.2% 15.0%	17	20.5% 85.0%	0	0% 0%
CA3b	208	94 (45.1%)	35	16.8% 37.2%	51	24.2% 54.3%	8	3.8% 8.5%
CA3c	103	33 (32.0%)	13	12.6% 39.4%	13	12.6% 39.4%	7	6.8% 21.2%
CA3 total	**394**	**147 (37.3%)**	**51**	**12.9% 34.7%**	**81**	**20.6% 55.1%**	**15**	**3.8% 10.2%**
CA1	**34**	**6 (17.7%)**						
DG	**82**	**26 (31.7%)**						

Both LFPg and CSD revealed two different types of SPW-Rs in the CA3 region (Fig. 1). Type 1 (T1) SPW-Rs ($n = 51/147$ SPW-Rs, CA3a: $n = 3/83$ slices, CA3b: $n = 35/208$ slices, and CA3c: $n = 13/103$ slices) were associated with a negative LFPg deflection in the pyramidal cell layer, and a positive LFPg deflection in the apical dendritic layer (stratum radiatum, Fig. 1A). In contrast, Type 2 (T2) SPW-Rs ($n = 81/147$ SPW-Rs, CA3a: $n = 17/83$ slices, CA3b: $n = 51/208$ slices, CA3c: $n = 13/103$ slices, Table 1) consisted of positive LFPg transients in the stratum (str.) pyramidale and the distal dendritic layer str. lacunosum-moleculare, with a correlated negative LFPg deflection in str. radiatum (Fig. 1B). CSD patterns of these two types of SPW-Rs also differed. T1 SPW-Rs showed a sink-source pair in the pyramidal cell layer, whereas T2 SPW-Rs displayed a source in the str. pyramidale and two sinks in the dendritic layers: str. oriens and radiatum (Fig. 1). The recurrence frequency of T1 SPW-Rs varied between 0.11 and 2.89 Hz with a mean ± SD of 1.12 ± 0.70 Hz (Table 2, Fig. 1C). That of T2 events was significantly higher (Mann–Whitney Rank Sum test, $P < 0.001$), with a mean of 1.62 ± 0.69 Hz and a range of 0.12–3.53 Hz. The amplitudes of T1 and T2 SPW-Rs measured in the str. pyramidale were −73.6 ± 67.5 μV and +43.7 ± 37.0 μV, respectively (significantly different, $P < 0.001$, Mann–Whitney Rank Sum test, Fig. 1D).

MUA and high frequency oscillations (especially ripple activity in the range of 150–300 Hz) increased during both types of SPW-Rs. During T1 SPW-Rs, MUA was 7.30 ± 8.57 μV (range 0.87–42.19 μV). During T2 SPW-Rs, MUA was 5.33 ± 7.27 μV (range, 0.33–52.01 μV). The difference in the MUA between T1 and T2 SPW-Rs was not statistically different ($P > 0.05$, Mann–Whitney Rank Sum test, Fig. 1E). Ripple activity could be detected in higher percentages of slices exhibiting T1 ($n = 41/45$ slices) than T2 ($n = 60/76$ slices) SPW-Rs. The average ripple power increase was somewhat higher during T1 (4.16 ± 9.31 μV^2; 3.36 ± 3.15 dB) than T2 SPW-Rs (2.32 ± 3.78 μV^2; 2.47 ± 1.93 dB, $P = 0.617$ for μV^2 scale, $P = 0.406$ for dB scale, Mann–Whitney Rank Sum test, Fig. 1F). The average frequency of ripples was similar: 197.2 ± 20.5 Hz during T1 and 192.8 ± 23.6 Hz during T2 SPW-Rs ($P = 0.337$, *t*-test). We found a clear positive correlation between the LFPg amplitude and the ripple power (dB) both in T1 ($R^2 = 0.2922$) and T2 ($R^2 = 0.1352$) SPW-Rs (as in Hájos et al., 2013).

In 15/147 of the cases, T1 and T2 SPW-Rs were simultaneously recorded (Fig. 2). This population pattern was generated only in the CA3b ($n = 8$) and CA3c ($n = 7$) subregions. In these cases, the frequency of T2 SPW-Rs was significantly higher than that of T1 SPW-Rs (0.56 ± 0.35 Hz vs. 1.57 ± 0.75 Hz, respectively, *t*-test, $P < 0.001$, Fig. 2C). The LFPg amplitude of T1 SPW-Rs (−122.0 ± 59.8 μV) was significantly different than that of T2 SPW-Rs (+34.1 ± 25.8 μV, Mann–Whitney Rank Sum test, $P < 0.001$). Plotting the LFPg amplitude of all SPW-Rs (both T1 and T2, detected on the same channel, located in the pyramidal cell layer) showed a clear two peak distribution (Fig. 2D). MUA was 14.54 ± 12.50 μV during T1, and 5.47 ± 8.02 μV during T2 SPW-Rs (Fig. 2B, significantly different, Mann–Whitney Rank Sum test, $P < 0.05$). Ripple power increase during T1 SPW-Rs was 14.66 ± 15.96 μV^2; 7.62 ± 2.79 dB ($n = 14/15$ slices) and was 4.00 ± 3.41 μV^2; 4.99 ± 2.59 dB during T2 SPW-Rs ($n = 12/15$ slices, significantly different both at μV^2 and dB scales, *t*-test, $P < 0.05$).

For the analysis of the SPW-Rs we used data from 33 animals (total number of slices: 274; 8.3 ± 2.1 slices/animals). We observed T1 SPW-Rs in 26/33 animals, T2 SPW-Rs in 29/33 animals and T1+T2 SPW-Rs in 11/33 animals. Altogether, we found CA3 SPW-Rs in 123/274 slices (47.9 ± 19.3% of slices per animal). There were no striking differences among animals concerning the occurrence of T1, T2, and T1+T2 SPW-Rs. SPW-Rs were observed in the CA3 region of all animals, although the percentage of slices exhibiting SPW-Rs varied between 16 and 85% (1/6 and 6/7 slices, respectively).

A set of experiments was performed to compare gradient and referential recordings. We made simultaneous recordings with two different systems on the same slices ($n = 28$ slices). One glass extracellular electrode was placed into the pyramidal cell layer of the CA3 region, with a reference electrode in the chamber, and SPW-Rs (in $n = 22/28$ slices, CA3a: $n = 5$, CA3b: $n = 12$, CA3c: $n = 5$) were recorded with a referential

ID: parasuramank Time: 14:11 I Path: N:/3b2/HIPO/Vol00000/140122/APPFile/JW-HIPO140122

J_ID: za4 Customer A_ID: HIPO22361 Cadmus Art: HIPO22361 Ed. Ref. No.: 13-341.R2 Date: 16-September-14 Stage: Page: 6

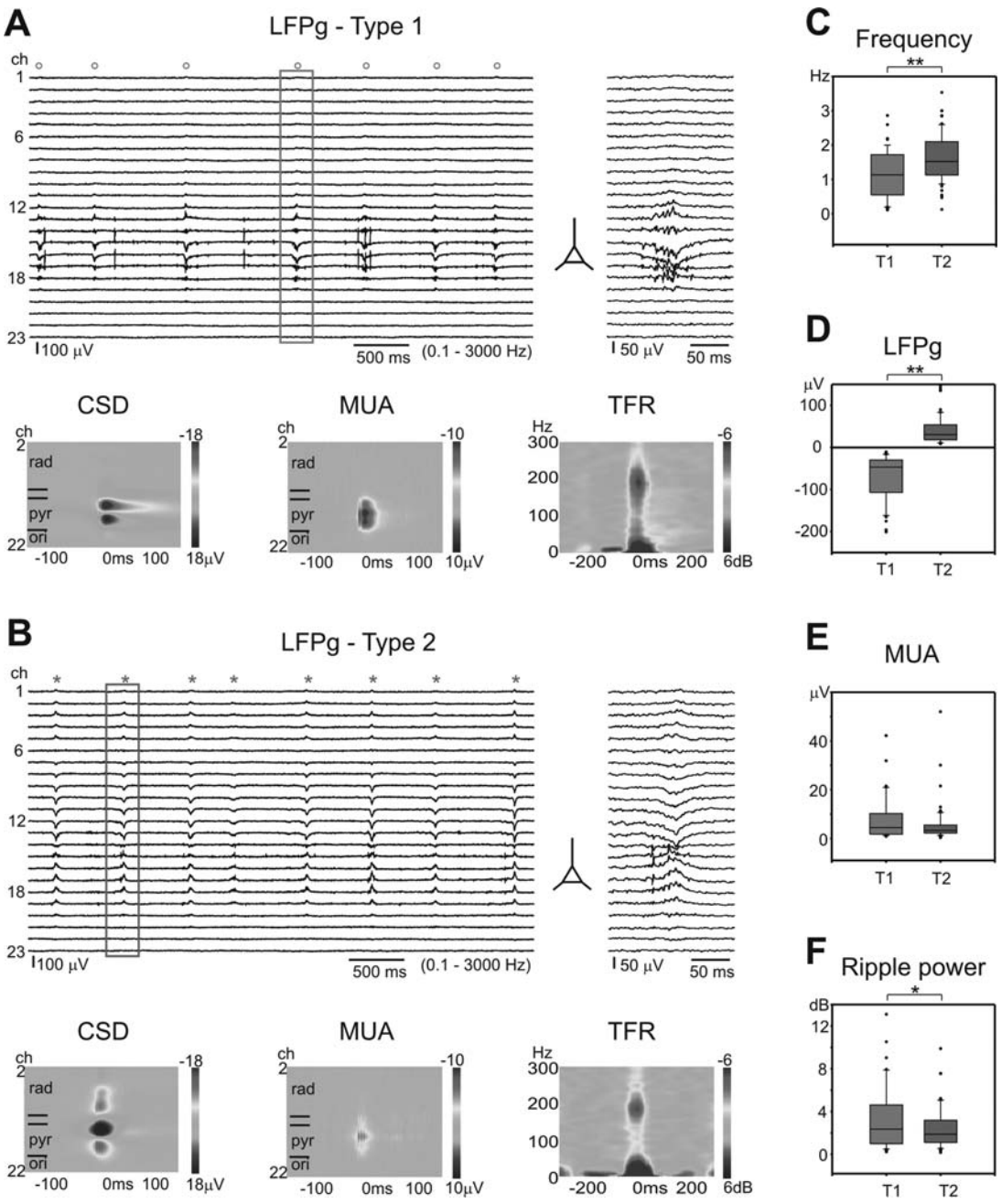

FIGURE 1. This figure shows the differences between T1 (A) and T2 (B) SPW-Rs. T1 SPW-Rs were characterized by a negative deflection whereas T2 by a positive deflection on the LFPg in the pyramidal cell layer (A, B, and D). SPW-Rs are marked with open circles (T1) and asterisks (T2), the SPW-Rs in the rectangles are magnified on the right side. Color maps show the CSD, the change in MUA of T1 (A) and T2 (B) SPW-Rs. A sink-source pair was found in the cell layer during T1 SPW-Rs, whereas a source was found in the str. pyramidale and two sinks were found in the strata radiatum and oriens during T2 SPW-Rs. Increased MUA was detected during both types of SPW-Rs. Note that MUA increase during T1 SPW-Rs was usually larger than during T2 SPW-Rs (A, B and E). Time frequency plots (TFR) demonstrate the presence of high frequency ripple oscillation both during T1 and T2 SPW-Rs. The recurrence frequency (C), the LFPg amplitude (D) and ripple power (F) of T1 and T2 SPW-Rs were found to be significantly different (*$P < 0.05$, **$P < 0.001$). On all figures, warm colors (red) depict current sink on the CSD maps and increase on the MUA and TFR maps. Cold colors (blue) depict current source on the CSD map and decrease on the MUA and TFR maps. On all figures mol, str. moleculare; gr, str. granulosum; h, hilus; rad, str. radiatum; pyr, str. pyramidale; ori, str. oriens. [Color figure can be viewed in the online issue, which is available at wileyonlinelibrary.com.] AQ2

ID: parasuramank Time: 14:11 I Path: N:/3b2/HIPO/Vol00000/140122/APPFile/JW-HIPO140122

J_ID: za4 Customer A_ID: HIPO22361 Cadmus Art: HIPO22361 Ed. Ref. No.: 13-341.R2 Date: 16-September-14 Stage: Page: 7

TABLE 2.

Basic Network Properties of SPW-R Activity in Different Pharmacological Experiments

		Recurrence frequency (Hz)	LFPg amplitude (μV)	MUA (μV)	Ripple power (dB)
T1 ($n = 51/147$)		1.12 ± 0.70	-73.6 ± 67.5	7.30 ± 8.57	3.36 ± 3.15
T2 ($n = 81/147$)		1.62 ± 0.69[a]	43.7 ± 37.0[a]	5.33 ± 7.27	2.47 ± 1.93
T1 + T2	T1 ($n = 15/147$)	0.56 ± 0.35	-121.99 ± 59.83	14.54 ± 12.50	7.62 ± 2.79
	T2 ($n = 15/147$)	1.57 ± 0.75[a]	34.11 ± 25.8[a]	5.47 ± 8.02[b]	4.99 ± 2.59[b]
APV	T1 control ($n = 5$)	1.55 ± 0.68	-56.0 ± 47.5	1.78 ± 1.63	
	T1 APV	1.71 ± 0.79	-60.6 ± 68.8	2.02 ± 2.04	
	T2 control ($n = 8$)	1.31 ± 0.57	49.8 ± 43.4	1.98 ± 1.68	
	T2 APV	1.44 ± 0.62	46.5 ± 34.3	2.40 ± 2.38	
CPG52432	T1 control ($n = 10$)	1.67 ± 0.87	-38.68 ± 40.35	1.02 ± 0.89	
	T1 CGP	1.66 ± 0.87	-32.29 ± 31.37	1.17 ± 1.17	
	T2 control ($n = 7$)	1.80 ± 0.99	48.51 ± 40.82	2.31 ± 1.77	
	T2 CGP	1.70 ± 0.65	34.92 ± 28.54	2.11 ± 1.63	
DCG-IV	T1 control ($n = 7$)	1.73 ± 0.75	-57.7 ± 77.8	4.29 ± 4.51	
	T1 DCG-IV	1.47 ± 0.50	-48.3 ± 59.1	3.05 ± 2.75	
	T2 control ($n = 7$)	1.21 ± 0.59	38.9 ± 19.3	2.18 ± 2.36	
	T2 DCG-IV	1.51 ± 0.43	63.8 ± 58.2	3.01 ± 3.71	
DAMGO	T1 control ($n = 14$)	1.28 ± 0.59	-80.3 ± 65.3	4.51 ± 7.15	2.21 ± 1.93
	T2 DAMGO	0.25 ± 0.16[a]	146.0 ± 194.3[a]	14.42 ± 30.60[b]	2.86 ± 2.03
	T2 control ($n = 26$)	1.18 ± 0.69	73.9 ± 52.0	3.80 ± 4.02	2.17 ± 1.74
	T2 DAMGO	0.13 ± 0.14[a]	101.4 ± 85.4 ($n = 12/26$)	7.33 ± 8.89[b] ($n = 12/26$)	3.36 ± 2.76

[a]Significantly different, $P < 0.001$
[b]significantly different, $P < 0.05$.

system (see Methods). The linear multielectrode was placed about 50–300 μm from the glass electrode (perpendicular to the cell layer), and SPW-Rs ($n = 22/28$ slices, CA3a: $n = 2$, border of CA3a/CA3b: $n = 3$, CA3b: $n = 15$, border of the CA3b/CA3c: $n = 5$) were recorded with the gradient recording system (see Methods). We recorded T1 ($n = 8$ slices) and T2 ($n = 14$ slices) SPW-Rs with the multiple channel gradient recording system. Simultaneously, the referential system recorded positive field potential deflections with similar waveforms during both T1 and T2 SPW-Rs, as well as high frequency oscillations and increased cellular activity (Fig. 2E). The average LFPg amplitude (mean ± SD) of T1 SPW-Rs was -98.64 ± 65.0 μV recorded with the gradient system, while the simultaneous field potential amplitude was 60.93 ± 25.65 μV detected with the referential system. The LFPg amplitude of T2 SPW-Rs was 73.22 ± 45.28 μV recorded with the gradient, and the field potential amplitude was 53.24 ± 33.40 μV recorded with the referential system. All values were measured in the pyramidal cell layer. Both types of SPW-Rs were detected in recordings made with the referential system. Their waveform was similar, and therefore they could only be distinguished in recordings performed with the multiple channel gradient system. The local field potential amplitude of T1 and T2 SPW-Rs recorded with the referential system showed no significant difference (t-test, $P = 0.585$). We have to note that both types of SPW-Rs showed somewhat larger amplitudes—measured with the gradient recording system—in the dual perfusion chamber (this set of experiments) than in the interface chamber (all other recordings, significantly not different, Mann–Whitney Rank Sum test, $P > 0.05$).

Role of Glutamatergic and GABAergic Signaling

We examined the role of glutamate and GABA signaling in the generation of SPW-R activity with antagonists of excitatory and inhibitory amino acid receptors (Figs. 3A,B). Both types of SPW-Rs were reversibly suppressed by either the AMPA/kainate glutamate receptor antagonist NBQX ($n = 5$ T1, $n = 8$ T2 SPW-Rs), or the $GABA_A$ receptor antagonist bicuculline ($n = 3$ T1, $n = 9$ T2 SPW-Rs), consistent with findings in other models (Papatheodoropoulos and Kostopoulos, 2002b; Maier et al., 2003; Behrens et al., 2005; Wu et al., 2005a,b; Ellender et al., 2010). The role of NMDA glutamate receptors in the generation of SPW-Rs is controversial. Several studies showed no changes in SPW-R amplitude and frequency when blocking NMDA receptors (Maier et al., 2003; Behrens et al., 2005; Wu et al., 2005a,b), whereas other work (Colgin et al., 2005; Ellender et al., 2010) demonstrated an increased amplitude and unchanged recurrence frequency of hippocampal SPW-Rs. Results observed in our model are closer to the first group of studies, the NMDA-receptor antagonist D,L-APV did not induce significant changes in the recurrence frequency, the LFPg amplitude or MUA of the two types of SPW-Rs ($n = 5$ T1, $n = 8$ T2, *t*-test or Mann–Whitney Rank Sum test,

ID: parasuramank Time: 14:11 I Path: N:/3b2/HIPO/Vol00000/140122/APPFile/JW-HIPO140122

J_ID: za4 Customer A_ID: HIPO22361 Cadmus Art: HIPO22361 Ed. Ref. No.: 13-341.R2 Date: 16-September-14 Stage: Page: 8

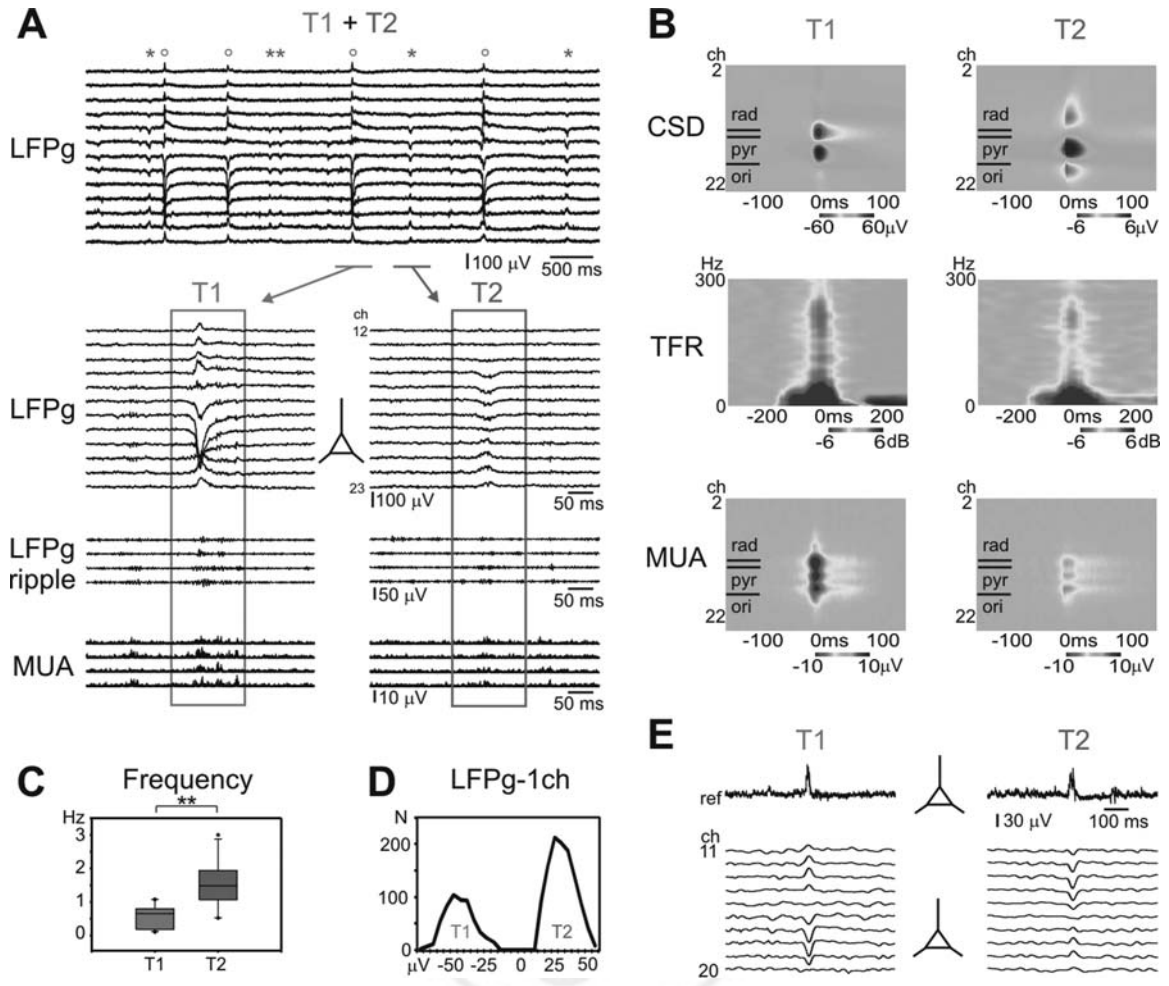

FIGURE 2. In 15/147 slices, T1 and T2 SPW-Rs were simultaneously generated in the CA3 region (A). Schematic pyramidal cell indicates the location of the cell layer and the orientation of the pyramidal cells. The LFPg amplitude (A), MUA increase (A, B) and ripple power (B) were significantly higher for T1 than for T2 SPW-Rs. Note the different scale for the CSD map. The recurrence frequency (C) of the two SPW-Rs was significantly different ($P < 0.001$). Plotting the LFPg amplitudes of the two types of SPW-Rs detected on one channel located in the pyramidal cell layer showed a clear two peak distribution (D). E) T1 and T2 SPW-Rs were indistinguishable in records made with referential system using one electrode placed in the pyramidal cell layer. Upper sweeps show the records made with the referential system (ref), lower sweeps are from the gradient recording (ch10-20, band pass filtered between 1 and 30 Hz). Schematic pyramidal cells show the location of the cell layer and the orientation of the pyramidal cells. [Color figure can be viewed in the online issue, which is available at wileyonlinelibrary.com.]**

$P > 0.05$, Table 2). We observed opposite tendencies than Colgin et al. (2005) and Ellender et al. (2010): D,L-APV slightly (but not significantly) increased the recurrence frequency of both types of SPW-Rs (T1: 110.5 ± 9.0% and T2: 115.2 ± 40.0% of control, Table 2), whereas the LFPg amplitude (T1: 96.8 ± 26.1%, T2: 98.7 ± 39.2%) and MUA (T1: 95.3 ± 52.4%, T2: 99.5 ± 33.3%) of both types of SPW-Rs remained unchanged. The $GABA_B$ receptor antagonist CGP52432 ($n = 10$ T1, $n = 7$ T2) did not change the frequency of SPW-Rs (T1: 99.8 ± 7.3%, T2: 100.7 ± 17.2% of control, Table 2). The LFPg amplitude of T1 SPW-Rs did not change (97.9 ± 38.1 % of control), while that of T2 SPW-Rs has decreased (to 69.0 ± 27.4% of control). The MUA of T1 and T2 SPW-Rs slightly increased (to 116.9 ± 51.8%) and decreased (to 90.0 ± 32.9%), respectively, in a bath solution containing CGP52432. None of the changes induced by CGP52432 were statistically different from the control (t-test or Mann–Whitney Rank Sum test, $P > 0.05$, Table 2).

Increasing extracellular K^+ concentration in vitro increases cellular excitability (Cohen and Miles, 2000). We used this approach to examine the impact of excitation on SPW-R activity. We investigated the network properties of T1 and T2 SPW-Rs in bathing medium with modified K^+ concentrations, over the range of 2−6 mM (see Supporting Information Fig. 3). In summary, the effect of 2 mM $[K^+]_e$ on the two types of SPW-R were different. The frequency of T1 events was greatly reduced, while that of T2 SPW-Rs was only slightly diminished. MUA decrease was significantly smaller during T2 SPW-Rs, than during T1 SPW-Rs. Increasing $[K^+]_e$ to 6 mM induced similar changes in T1 and T2 SPW-Rs: an increase in

ID: parasuramank Time: 14:11 I Path: N:/3b2/HIPO/Vol00000/140122/APPFile/JW-HIPO140122

J_ID: za4 Customer A_ID: HIPO22361 Cadmus Art: HIPO22361 Ed. Ref. No.: 13-341.R2 Date: 16-September-14 Stage: Page: 9

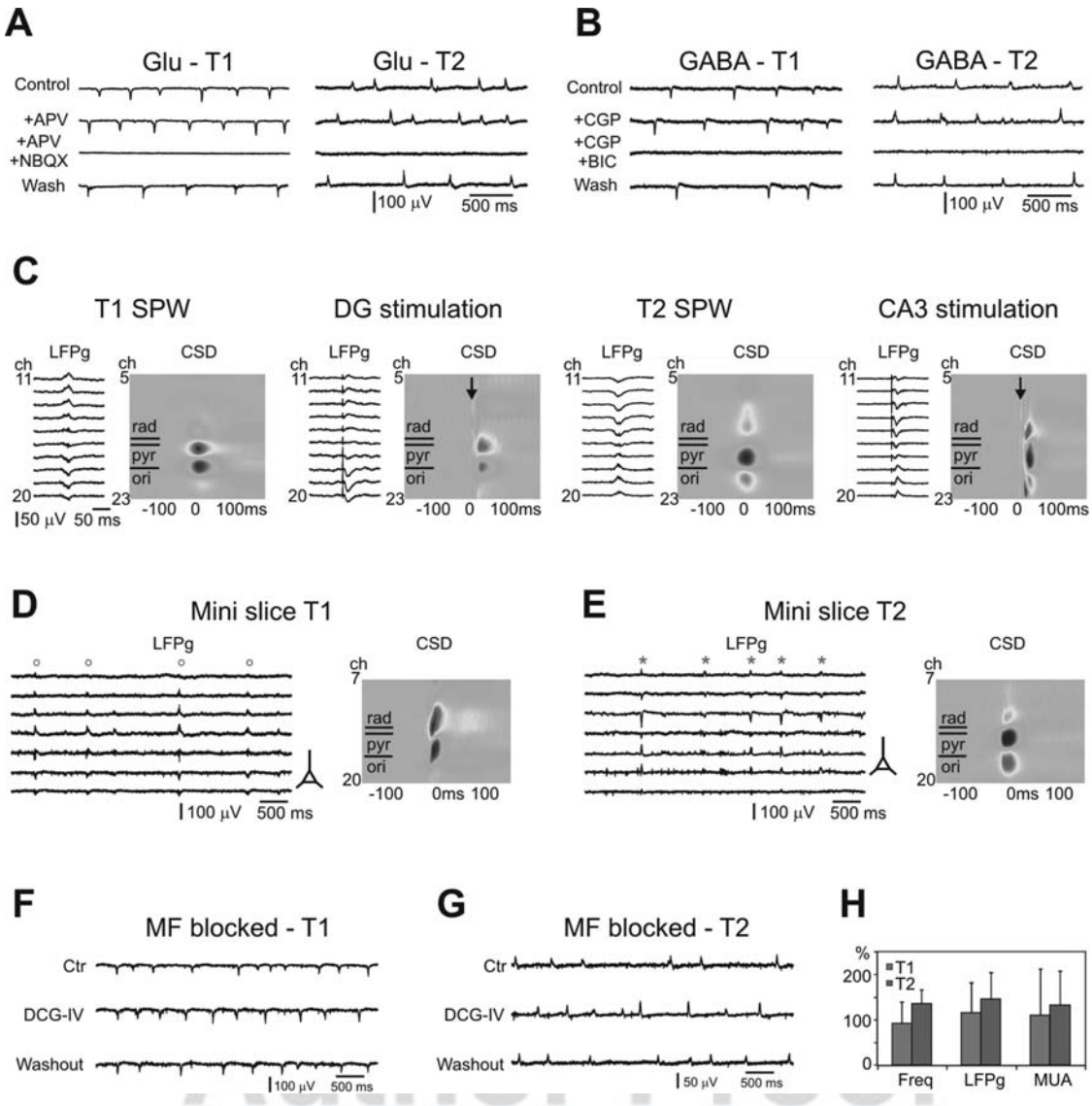

FIGURE 3. SPW-Rs depend on both glutamatergic (A) and GABAergic (B) signaling. The application of the NMDA antagonist D,L-APV did not significantly alter T1 and T2 SPW-Rs, while the AMPA/kainate receptor antagonist NBQX reversibly blocked them (A). The $GABA_B$ receptor CGP52432 did not significantly changed the SPW-Rs, whereas the $GABA_A$ receptor antagonist bicuculline (BIC) reversibly blocked the population events (B). Stimulation of the DG and CA3 recurrent collaterals evoked slightly different responses than spontaneous T1 and T2 SPW-Rs, respectively (C). Left panels show the LFPg recorded in the proximal dendritic and somatic layers (channels 11–20), right panels show the CSD maps of the entire CA3 region. Arrows depict the stimulation artifacts on the CSD maps. Both types of SPW-Rs were detected in mini slices comprising the CA3 region only (T1 SPW-Rs on D, T2 SPW-Rs on E). Schematic pyramidal cells show the location of the cell layer and the orientation of the pyramidal cells. Blockade of mossy fiber (MF) release by bath application of the mGluR2 agonist DCG-IV did not suppress the emergence of T1 (F) or T2 (F) SPW-Rs in the CA3 region. The recurrence frequency (Freq) of T1 SPW-Rs slightly decreased, while that of T2 SPW-Rs increased (F). On average, the LFPg amplitude and MUA of both types of SPW-Rs increased with a high variability (F) during application of DCG-IV. [Color figure can be viewed in the online issue, which is available at wileyonlinelibrary.com.]

frequency of about 30%, a reduction in amplitude of about 20–30%, and an increase in MUA of about 25%.

Role of Excitatory Pathways in the Generation of SPW-Rs

The CSD pattern of T1 and T2 SPW-Rs recalled the activation pattern of mossy fibers (MFs) and CA3 recurrent collaterals, respectively (Fig. 3C). To explore whether these excitatory pathways participate in the generation of SPW-Rs, we made three sets of experiments. First, we stimulated both MFs and CA3 recurrent collaterals in slices with spontaneous T1 ($n = 5$) and T2 ($n = 6$) SPW-Rs. When stimulating MFs we found an activation pattern that was only slightly different from the one observed during spontaneous T1 SPW-Rs (Fig. 3C left side). The sink representing MF activation was shifted by about 50

ID: parasuramank Time: 14:12 I Path: N:/3b2/HIPO/Vol00000/140122/APPFile/JW-HIPO140122

J_ID: za4 Customer A_ID: HIPO22361 Cadmus Art: HIPO22361 Ed. Ref. No.: 13-341.R2 Date: 16-September-14 Stage: Page: 10

TABLE 3.

Resting Membrane Potential (RMP) and Cellular Responses to SPW-Rs of Intracellularly Recorded Putative CA3 Pyramidal Cells

		Response to	
Number of cells	RMP (mV)	T1 SPW	T2 SPW
6	−54.3 ± 4.6	hyperpolarizing	
1	−71.0	biphasic	
18	−60.6 ± 7.5		hyperpolarizing
2	−53.4 ± 0.5		biphasic
2	−56.2 ± 3.5		depolarizing
8	−57.3 ± 3.4	hyperpolarizing	hyperpolarizing
4	−61.4 ± 5.9	biphasic	biphasic
1	−60.8	depolarizing	depolarizing
1	−60.3	depolarizing	hyperpolarizing
Total $n = 43$	−58.9 ± 6.4		

μm toward the fissure (in the str. lucidum), compared to the sink of T1 SPW-R (being in the upper part of the str. pyramidale). The source of the evoked response was also shifted by about 50 μm toward str. oriens compared to the source of the spontaneous SPW-Rs. Stimulation of CA3 recurrent collaterals also activated somewhat different transmembrane currents than spontaneous T2 SPW-Rs: the sinks in the str. oriens and radiatum were about 50 μm closer to the pyramidal cell layer (Fig. 3C right side), than during T2 SPW-Rs. In summary, activation pattern of MFs and CA3 recurrent collateral stimulation resembled to T1 and T2 SPW-Rs, respectively, but they were not identical.

Since MF activation resulted in a similar but distinguishable pattern as in spontaneous T1 SPW-Rs, we made further experiments to clarify whether the activity of dentate granule cells is required for the generation of T1 SPW-Rs. Therefore, we made recordings in the CA3 region in slices where intrahippocampal connections were cut. If MF activation is necessary to the generation of SPW-Rs, the lack of transmission between granule cells and CA3 cells would prevent the emergence of SPW-Rs. In contrast to this hypothesis, both types of SPW-Rs were found in CA3 mini slices ($n = 9$ slices, Figs. 3D–F). In one slice, T1+T2 SPW-Rs were simultaneously recorded, both in the CA3a and CA3b regions. The CA3a region of another slice generated T2 SPW-Rs, while T1 SPW-Rs were recorded in the CA3b region of the same slice. In three slices T1 ($n = 2$ in CA3a and $n = 1$ in CA3b), and in 4 slices T2 SPW-Rs were detected ($n = 1$ in CA3a and $n = 3$ in CA3b).

In the third set of experiments, we explored the role of the dentate gyrus in the initiation of CA3 SPW-Rs by blocking the glutamate release from MFs with the mGluR2 agonist DCG-

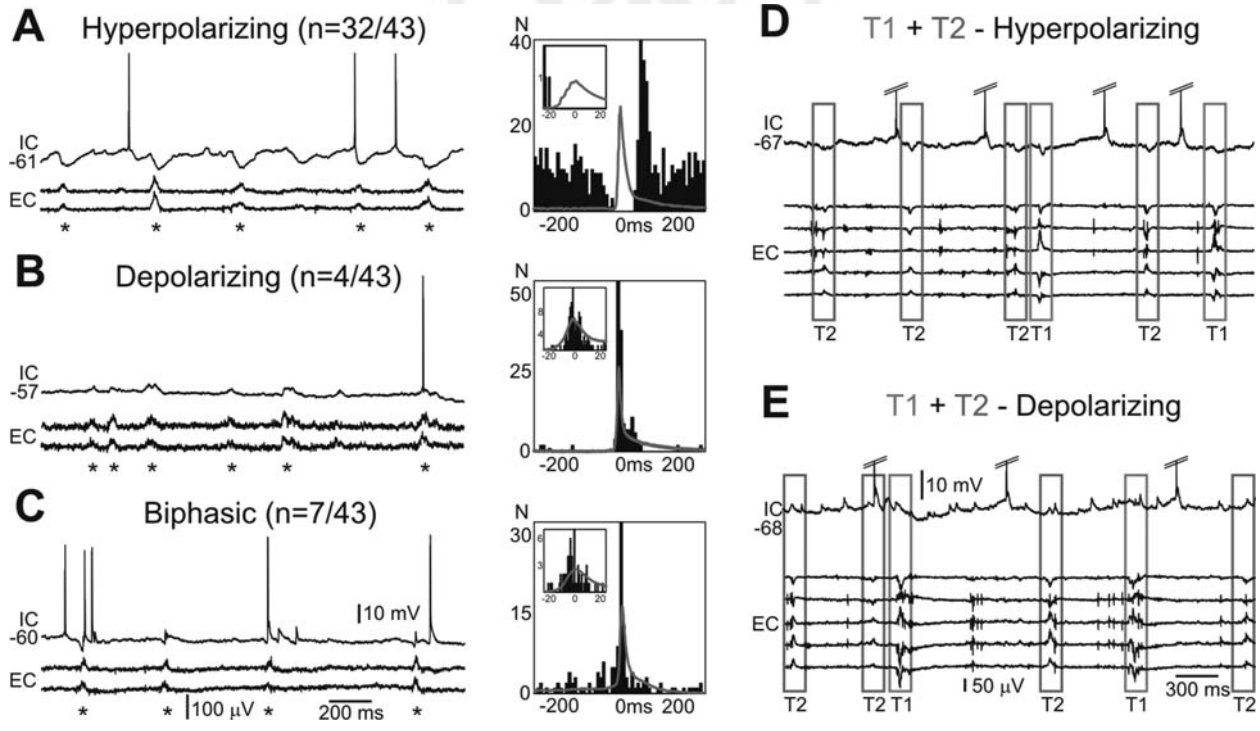

FIGURE 4. Putative pyramidal cells showed three different behaviors during SPW-Rs, as revealed by intracellular recordings (A–C). Left panels illustrate intracellular (IC) and two channels of extracellular (EC) records. Right panels show cell firing histograms compared to SPW-Rs. LFPg averages of the SPW-Rs are indicated by red lines on the histograms. The majority of the cells were hyperpolarized (A) and ceased firing during SPW-Rs (asterisks). About 10% of the cells were purely depolarized (B) and discharged during SPW-Rs. Several cells showed a biphasic response (hyperpolarization and depolarization) to SPW-Rs (C). Three of the biphasic cells reliably increased their firing during SPW-Rs. Some cells showed hyperpolarizing (D) or depolarizing (E) responses to both types of SPW-Rs. [Color figure can be viewed in the online issue, which is available at wileyonlinelibrary.com.]

ID: parasuramank Time: 14:12 I Path: N:/3b2/HIPO/Vol00000/140122/APPFile/JW-HIPO140122

J_ID: za4 Customer A_ID: HIPO22361 Cadmus Art: HIPO22361 Ed. Ref. No.: 13-341.R2 Date: 16-September-14 Stage: Page: 11

IV (Kamiya et al., 1996). Contrary to previous findings (Rex et al., 2009) showing that bath application of DCG-IV largely reduced the incidence of SPW-Rs, we found only a slightly diminished occurrence frequency of T1 SPW-Rs ($n = 7$, $92.1 \pm 46.3\%$, see also), and an increased frequency of T2 SPW-Rs ($n = 7$, $135.4 \pm 30.6\%$, Table 2). The change in LFPg amplitude was highly variable to the bath application of DCG-IV: it decreased for T1 SPW-Rs in $n = 4/7$ and increased in $n = 3/7$ slices, and decreased for T2 SPW-Rs in $n = 1/7$ and increased in $n = 6/7$ slices. On average, DCG-IV increased the LFPg amplitude of both T1 ($115.2 \pm 66.2\%$) and T2 ($146.0 \pm 58.0\%$) SPW-Rs (Table 2). Applying DCG-IV slightly increased the MUA of both T1 ($109.6 \pm 102.1\%$), and T2 ($132.1 \pm 74.9\%$) SPW-Rs, with a very high variability (Figs. 3F–H, Table 2). None of the changes were significant ($P > 0.05$, *t*-test for the frequency, Mann–Whitney Rank Sum test for LFPg amplitude and MUA).

In summary, spontaneous T1 and T2 SPW-Rs showed a slightly different CSD pattern than mossy fiber or CA3 recurrent collateral stimulation, respectively. Either suppression of mossy fiber transmitter release or cutting intrahippocampal connections did not block the emergence of T1 or T2 SPW-Rs in the CA3 region.

Cellular Responses to SPW-Rs

In earlier works, considerably different results were obtained concerning the cellular responses of CA3 pyramidal cells during SPW-Rs. The importance of either hyperpolarizing (Wu et al., 2005b; Hájos et al., 2009) or depolarizing (Colgin et al., 2004a) or both types of responses were emphasized (Behrens et al., 2005). Furthermore, depolarizing, hyperpolarizing, mixed synaptic potentials and no responses were shown to occur in the same CA3 pyramidal cell during SPW-R activity (Ellender et al., 2010). Simultaneous intra- and extracellular recordings were made from the CA3 pyramidal cell layer to examine the cellular correlates of SPW-Rs in our slice model. We recorded from 43 putative CA3 pyramidal cells located in the CA3a ($n = 5$), CA3b ($n = 32$) and CA3c ($n = 6$) regions. Pyramidal cell resting membrane potential was -58.9 ± 6.3 mV, input resistance was 23.7 ± 9.4 MΩ, and time constant was 19.5 ± 8.7 ms.

Recordings were made from 7 cells in slices where T1 SPW-Rs were generated, from 22 cells with T2 and from 14 cells in slices with both T1 and T2 SPW-Rs. Pyramidal cells were hyperpolarized ($n = 32$) depolarized ($n = 4$) or showed a biphasic (hyperpolarizing-depolarizing, $n = 7$) response during SPW-Rs (Table 3, Supporting Information Table 1, Fig. 4; cf Maier et al., 2003; Behrens et al., 2005). At resting potential, cells responded to consecutive SPW-Rs with similar hyperpolarizing or depolarizing events. Fourteen cells were recorded during both types of SPW-R: 12 of them were hyperpolarized (Fig. 4D) and one cell was depolarized during both types of SPW-R (Fig. 4E). One cell depolarized during T1 SPW-Rs, and hyperpolarized during T2 SPW-Rs (Table 3). The SPW-R associated events, in a subgroup of pyramidal cells, consisted of a depolarizing event superimposed on a primarily hyperpolarizing response ($n = 7$ cells, Fig. 4C). All events consisted of such biphasic (hyperpolarizing–depolarizing) potentials in just one cell. In most cells ($n = 6$), a depolarizing component was associated with most, but not all, SPW-Rs ($79.3 \pm 14.2\%$). When the same slice generated both T1 and T2 SPW-Rs, the depolarizing component of biphasic responses ($n = 4$ cells) was much more often associated with T1 ($78.3 \pm 17.6\%$), than with T2 ($11.1 \pm 4.5\%$) SPW-Rs.

The ratio of cells showing hyperpolarizing/depolarizing/biphasic responses to T1 and to T2 SPW-Rs was slightly different. Out of 21 cells recorded together with T1 SPW-Rs 14 showed hyperpolarizing (66.7%), 5 biphasic (23.8%) and 2 depolarizing (9.5%) responses, whereas out of 36 cells with simultaneously detected T2 SPW-Rs 27 responded with hyperpolarizing (75.0%), 6 with biphasic (16.7%), and 3 with depolarizing (8.3%) potentials (Table 3).

At resting potential, 9 of the 43 pyramidal cells fired during SPW-Rs (Supporting Information Table 1). All of these cells showed depolarizing or biphasic synaptic events in response to SPW-Rs. High percentages of depolarizing and biphasic cells fired during SPW-Rs ($n = 9$ of 11 cells), although with variable reliability. Five of the 9 cells discharged quite rarely, in $3.4 \pm 1.5\%$ of SPW-Rs, while 4 of the 9 cells discharged more reliably, in $38.4 \pm 30.1\%$ of SPW-Rs (2 and 2 related with T1 and T2 SPW-Rs). Five out of 21 cells (23.8%) fired during T1, and 6/36 cells (16.7%) discharged during T2 SPW-Rs.

Next, an estimation of excitatory and inhibitory input was investigated by two different analyses (Supporting Information Fig. 4). The reversal potential of synaptic events associated with SPW-Rs was found to be similar in T1 and T2 SPW-Rs. The amplitude of cellular responses at different holding potentials was somewhat larger (although not significantly different) in relation with T1 than T2 SPW-Rs (Supporting Information Table 1).

Ectopic action potentials (eAPs) observed in CA1 pyramidal cells were suggested to have a possible role in the formation of oscillating assemblies (Papatheodoropoulos, 2008; Bahner et al., 2011). We examined the presence of eAPs in our intracellular recordings as well as their possible relationship with T1 and T2 SPW-Rs (Supporting Information Fig. 5). Interestingly, the occurrence of ectopic APs and bursts was considerably related to cells showing either depolarizing or biphasic responses ($n = 7/7$ biphasic, $n = 2/4$ depolarizing and $n = 3/32$ hyperpolarizing cells). We could not demonstrate considerable differences between T1 and T2 SPW-Rs regarding the presence of eAPs.

In summary, cells responded to SPW-R activity with either hyperpolarizing, depolarizing, or biphasic responses. Two thirds and three quarters of neurons showed hyperpolarizing responses to T1 and T2 SPW-Rs, respectively. Slightly more cells discharged during T1 than T2 SPW-Rs, with variable reliability. The depolarizing component of biphasic responses was more often associated with T1, than with T2 SPW-Rs.

ID: parasuramank Time: 14:12 I Path: N:/3b2/HIPO/Vol00000/140122/APPFile/JW-HIPO140122

J_ID: za4 Customer A_ID: HIPO22361 Cadmus Art: HIPO22361 Ed. Ref. No.: 13-341.R2 Date: 16-September-14 Stage: Page: 12

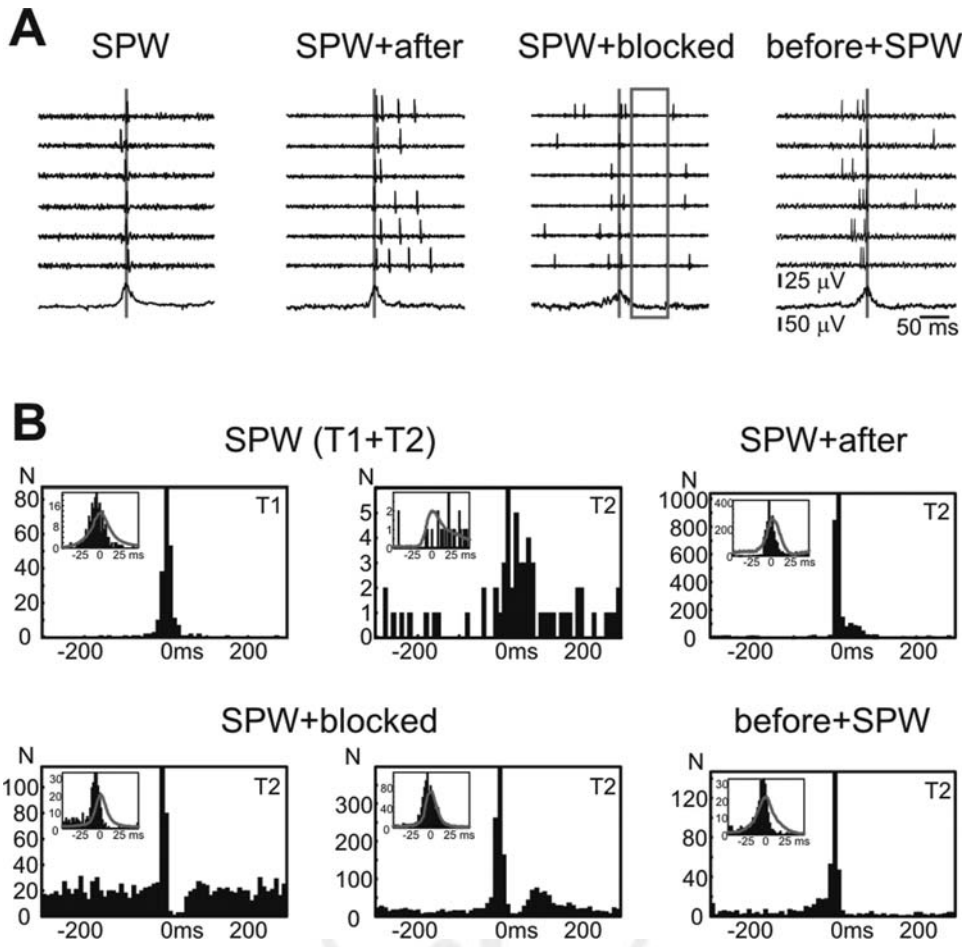

FIGURE 5. Interneurons of the CA3 region increased their firing rate during SPW-Rs with four different patterns (A). Consecutive sweeps of interneuron firing (upper traces, 500–3,000 Hz) and one representative LFPg trace of SPW-Rs (lower trace 0.1–500 Hz) are shown. B) Histogram of interneuron firing relative to the SPW-Rs. LFPg averages of the SPW-Rs are indicated by red lines. The same interneuron can show different timing to the two types of SPW-Rs: SPW (T1+T2). "SPW+blocked" class of interneurons was found only in the str. oriens and could be divided into two subclasses, one without (left), the other with (right) a rebound firing after the silent period. "SPW+after" and "before+SPW" firing patterns were only observed in relation with T2, but not T1 SPW-Rs. The maximal firing of the majority of the cells ($n = 53/71$) preceded the LFPg peak of the SPW-Rs. [Color figure can be viewed in the online issue, which is available at wileyonlinelibrary.com.]

Role of Interneurons

Our data show that high proportions of pyramidal cells are inhibited during SPW-Rs, consistent with previous findings (Wu et al., 2005a,b). We asked how selected interneurons discharge during SPW-Rs by searching for single unit extracellular activity in the CA3 region (see Methods). Reliable single-unit activity was recorded from 71 putative interneurons: 31 cells in str. oriens, 24 cells in the str. pyramidale, 13 cells in str. lucidum and radiatum, 2 cells in str. lacunosum-moleculare (str. lac-mol), and 1 cell in the hilus (Table 4, Fig. 5). The firing of 16 interneurons was compared to the timing of T1 SPW-Rs, discharges of 38 interneurons were compared to T2 SPW-Rs, and 17 putative interneurons with both SPW-R types.

Interneurons located in the str. oriens showed higher average firing rate than cells situated in other layers. Furthermore, cells related to T2 SPW-Rs discharged with a higher rate than interneurons associated with T1 or with T1+T2 SPW-Rs in all layers. None of these differences were statistically significant although (ANOVA on Ranks, $P > 0.05$)

Peri-event time histograms (PETH) were constructed to compare the timing of interneuron firing with SPW-R occurrence. We detected five different patterns of interneuron firing behavior (Tables 4–6, Fig. 5). (1) increased firing during SPW-Rs ("SPW", $n = 39$ cells); (2) increased firing, followed by a reduction or cessation of firing ("SPW+blocked", $n = 9$ cells); (3) increased firing, followed by lesser persistent firing ("SPW+after", $n = 14$ cells); (4) some increase in firing before SPW-R onset followed by a larger increase ("before+SPW", $n = 3$ cells); and (5) firing unrelated to SPW-Rs ("not related", $n = 15$ cells). In the "SPW+blocked" groups, we distinguished 6 cells showing a rebound firing increase after the silence and 3 cells with no rebound (Fig. 5B). Tables 5 and 6 show numbers and locations within the CA3 region of cells with different

ID: parasuramank Time: 14:12 I Path: N:/3b2/HIPO/Vol00000/140122/APPFile/JW-HIPO140122

J_ID: za4 Customer A_ID: HIPO22361 Cadmus Art: HIPO22361 Ed. Ref. No.: 13-341.R2 Date: 16-September-14 Stage: Page: 13

TABLE 4.

Number, Location, and Firing Rate of Clustered Interneurons Relative to the Occurrence of Different SPW-R Patterns

	Total		T1 SPW-R		T2 SPW-R		T1+T2 SPW-R	
	Number of cells	Firing rate (Hz)	Number of cells	Firing rate (Hz)	Number of cells	Firing rate (Hz)	Number of cells	Firing rate (Hz)
Str. oriens	31	3.6 ± 4.0	8	1.7 ± 1.9	21	4.7 ± 4.4	2	0.8 ± 0.4
Str. pyramidale	24	1.8 ± 2.8	5	0.4 ± 0.3	8	2.7 ± 4.5	11	2.0 ± 1.4
Str. lucidum+radiatum	13	1.7 ± 2.1	3	1.6 ± 0.2	8	2.0 ± 2.6	2	0.9 ± 0.7
Str. lacunosum-moleculare	2	1.7 ± 0.3			1	1.48	1	2.0
Hilus	1	1.5					1	1.5
Total	71	2.5 ± 3.3	16	1.3 ± 1.4	38	3.6 ± 4.1	17	1.5 ± 1.1

behaviors as well as the type of SPW-R with which their firing was compared.

Interneuron firing patterns during T1 and T2 SPW-Rs were different. While the numbers of interneurons showing "SPW", "SPW+blocked" and "not related" behaviors were comparable for both types of SPW-Rs, no cells showed "SPW+after" or "before+SPW" firing patterns during T1 SPW-Rs (Tables 5 and 6). Interneurons recorded from different layers of the CA3 region behaved differently. Cells with a "SPW+blocked" firing pattern were detected only in str. oriens. Neurons of the other groups were detected with similar frequencies in the different layers (Table 6). Furthermore, we observed 10 out of 17 interneurons with different firing behavior relative to the two SPW-R types. One cell recorded from the str. oriens fired with "SPW+blocked" pattern during T1 and "SPW" during T2 SPW-Rs, 2 cells located in str. lucidum+radiatum showed "SPW" pattern to T1 and "SPW+after" to T2 SPW-Rs, the hilar interneuron and 2 cells in the str. pyramidale showed "SPW" pattern to T1, but their firing was unrelated to T2 SPW-Rs, the remaining cells in str. pyramidale showed "not related" to T1 and "SPW" ($n = 3$) or "SPW+after" ($n = 1$) pattern to T2 SPW-Rs.

PETH analysis let us determine the timing of maximal interneuron firing relative to SPW-Rs (see Methods, Tables 5 and 6). Most interneurons fired 5–10 ms before the peak of the LFPg associated with a SPW-R. For all cells ($n = 71$), the mean time difference was -3.1 ± 9.5 ms. Mean differences with respect to T1 and T2 SPW-Rs were -5.5 ± 5.2 ms and -1.6 ± 11.2 ms, respectively (statistically not different, Mann–Whitney Rank Sum test, $P > 0.05$). Neurons of the "SPW+after" group fired 1.2 ± 13.3 ms after the SPW-R field peak (Table 5), while cells of other groups discharged about 5 ms before the LFPg peak (significantly not different, ANOVA on Ranks, $P > 0.05$). The timing of cell firing in the groups "SPW" and "SPW+blocked" was similar with respect to T1 and T2 SPW-Rs (Mann–Whitney Rank Sum test, $P > 0.05$).

Interneurons of different layers fired with different timing with respect to SPW-R fields. Cells recorded from str. oriens fired significantly earlier (-5.5 ± 5.5 ms) than cells in str. pyramidale (-1.6 ± 8.5 ms) or str. lucidum/radiatum (2.1 ± 13.3 ms, ANOVA on Ranks, $P < 0.05$), compared with the SPW-R peaks. The 2 cells in the str. lucidum/radiatum showing "SPW" and "SPW+after" behavior to T1 and T2 SPW-Rs (see above) fired before T1 SPW-Rs (by -10.2 and -4.2 ms), but after the peak of T2 SPW-Rs (by 22.3 and 39.3 ms).

In summary, the firing of nearly all interneurons increased in association with SPW-Rs. Several different discharge patterns were observed. Nearly two thirds of the recorded interneurons

TABLE 5.

Number of interneurons with different behaviors and timing of their maximal firing relative to the two types of SPW-Rs, as well as their firing rate.

	Total			T1 SPW-R			T2 SPW-R		
Behavior	Number of cells	Timing to SPW-R (ms)	Firing rate (Hz)	Number of cells	Timing to SPW-R (ms)	Firing rate (Hz)	Number of cells	Timing to SPW-R (ms)	Firing rate (Hz)
SPW	39	−3.7 ± 9.0	1.7 ± 2.3	24	−5.3 ± 5.1	1.4 ± 1.3	21	−1.8 ± 11.9	2.2 ± 2.8
SPW + blocked	9	−5.9 ± 3.9	5.2 ± 4.9	3	−6.6 ± 7.2	1.1 ± 0.5	6	−5.5 ± 1.9	7.3 ± 4.8
SPW + after	14	1.2 ± 13.3	3.9 ± 4.0				14	1.2 ± 13.3	3.9 ± 4.0
Before + SPW	3	−4.7 ± 1.0	1.4 ± 0.7				3	−4.7 ± 1.0	1.4 ± 0.7
not related	15	N/A	1.3 ± 1.2	6	N/A	1.7 ± 1.4	11	N/A	0.9 ± 1.0
Total	71	−3.1 ± 9.5	2.5 ± 3.3	33	−5.5 ± 5.2	1.4 ± 1.3	55	−1.6 ± 11.2	2.9 ± 3.6

ID: parasuramank Time: 14:12 I Path: N:/3b2/HIPO/Vol00000/140122/APPFile/JW-HIPO140122

J_ID: za4 Customer A_ID: HIPO22361 Cadmus Art: HIPO22361 Ed. Ref. No.: 13-341.R2 Date: 16-September-14 Stage: Page: 14

TABLE 6.

Number of Interneurons with Different Behaviors Relative to Their Location, and Their Timing to the Different SPW-Rs

	Str. oriens		Str. pyramidale		Str.lucidum/ radiatum		Str. lacunosum-moleculare	
Behavior	Timing to T1 SPW-R (ms)	Timing to T2 SPW-R (ms)	Timing to T1 SPW-R (ms)	Timing to T2 SPW-R (ms)	Timing to T1 SPW-R (ms)	Timing to T2 SPW-R (ms)	Timing to T1 SPW-R (ms)	Timing to T2 SPW-R (ms)
SPW	-6.5 ± 1.7 $n = 7$	-5.9 ± 11.3 $n = 6$	-5.8 ± 6.2 $n = 11$	5.3 ± 9.0 $n = 8$	-2.8 ± 5.8 $n = 4$	-2.2 ± 5.3 $n = 6$	-7.9 $n = 1$	-32.9 $n = 1$
SPW + blocked	-6.6 ± 7.2 $n = 3$	-5.5 ± 1.9 $n = 6$						
SPW + after		-3.8 ± 3.0 $n = 7$		-3.8 ± 3.8 $n = 4$		19.3 ± 21.7 $n = 3$		
Before + SPW not related		-5.8 $n = 1$ $n = 3$	$n = 4$	$n = 4$	$n = 1$	-4.3 $n = 1$		-4.0 $n = 1$
Total	-6.6 ± 3.7 $n = 10$	-5.0 ± 6.2 $n = 23$	-5.9 ± 6.2* $n = 15$	2.3 ± 8.7* $n = 16$	-2.8 ± 5.8 $n = 5$	4.1 ± 15.2 $n = 10$	-7.9 $n = 1$	-18.5 ± 20.4 $n = 2$

($n = 53/71$) fired maximally before the peak of SPW-R fields. Interneuron firing patterns varied according to their location and the type of the SPW-R. About 60% of neurons recorded during T1+T2 SPW-R activity ($n = 10/17$) showed different firing patterns to the two types of SPW-Rs.

Role of Perisomatic Interneurons

Perisomatic inhibitory cells were found to have an important role in the initiation of SPW-Rs in vitro (Ellender et al., 2010; Hájos et al., 2013). In our model, a CSD source was detected in the CA3 pyramidal layer during both types of SPW-Rs. The ratio of hyperpolarizing pyramidal cells also supports the hypothesis that these are active inhibitory transmembrane currents, possibly mediated by perisomatic interneurons. To explore this question, we reduced the activity of PV-positive basket cells and somatostatin-positive dendritic inhibitory cells using the mu opioid receptor agonist DAMGO (Drake and Milner, 2002; Gulyás et al., 2010). We added 1 μM DAMGO to the bathing medium in 14 slices with T1, in 26 slices with T2 and in 4 slices with T1+T2 SPW-Rs. As it has been reported recently in the CA1 region (Giannopoulos and Papatheodoropoulos, 2013), the recurrence frequency was considerably reduced in all slices (T1: $22.6 \pm 24.2\%$; and T2: $11.5 \pm 14.3\%$, significantly different, $P < 0.001$, Mann–Whitney Rank Sum test, Table 2, Figs. 6A,B). The LFPg and CSD pattern of T1 SPW-Rs has been reversibly converted into T2 SPW-Rs ($n = 11/14$, Fig. 6C) or to undefined pattern ($n = 3/14$) during DAMGO application. The CSD pattern of T2 SPW-Rs remained unchanged (i.e., source in the pyramidal layer and two sinks in the dendritic layers) in 14/26 slices (Fig. 6D), whereas DAMGO reversibly blocked T2 SPW-R activity in 12/26 slices. In two of four slices with both T1 and T2 SPW-Rs only T2 SPW-Rs (Fig. 6E) were detected during application of DAMGO, whereas in the two other slices SPW-Rs with undefined pattern were present. The LFPg amplitude of T1 SPW-Rs changed from -80.3 ± 65.3 μV in control to 146.0 ± 194.3 μV in DAMGO (significantly different, $P < 0.001$, Mann–Whitney Rank Sum test). The LFPg amplitude of T2 SPW-Rs increased from 73.9 ± 52.0 μV in control to 101.4 ± 85.4 μV in DAMGO ($152.1 \pm 98.8\%$, significantly not different, $P > 0.05$, Mann–Whitney Rank Sum test). The MUA of both types of SPW-Rs significantly increased (T1: from 4.51 ± 7.15 μV in control to 14.42 ± 30.60 μV in DAMGO, $376.6 \pm 308.7\%$; T2: from 3.80 ± 4.02 μV in control to 7.33 ± 8.89 μV in DAMGO, $215.6 \pm 136.2\%$, both significantly different, $P < 0.05$, Mann–Whitney Rank Sum test), with a high variability (Table 2, Figs. 6A,B). In contrast to findings in the CA1 region (Giannopoulos and Papatheodoropoulos, 2013), a significant increase (of about 100% on average) was found in the ripple power of all SPW-Rs during DAMGO application (Mann–Whitney Rank Sum test, $P < 0.05$). Ripple power of T1 SPW-Rs changed from 2.21 ± 1.93 dB in control (T1) to 2.86 ± 2.03 dB in DAMGO (T2), and ripple power of T2 SPW-Rs was modified from 2.17 ± 1.74 dB in control (T2) to 3.36 ± 2.76 dB in DAMGO (T2). The average frequency of the ripples remained similar: it changed from 201.74 ± 24.91 Hz to 211.92 ± 33.56 Hz ($106.2 \pm 22.3\%$) in T1 SPW-Rs, and from 206.49 ± 26.81 Hz to 204.49 ± 26.81 Hz ($101.3 \pm 14.2\%$) in T2 SPW-Rs. These changes were not statistically significant (t-test or Mann–Whitney Rank Sum test, $P > 0.05$). The SPW-R LFPg amplitude and the ripple power showed positive correlation in these experiments as well, in agreement with previous findings (see above and Hájos et al., 2013).

Next, we examined the effect of DAMGO on individual inhibitory cells. We clustered several interneurons located in the str. oriens ($n = 11$) and pyramidale ($n = 23$). As expected (Drake and Milner, 2002; Gulyás et al., 2010), interneurons responded by either increasing ($n = 9$) or decreasing ($n = 25$) their firing rate during DAMGO application. The firing pattern during SPW-Rs either remained unchanged ($n = 18$ cells),

ID: parasuramank Time: 14:12 I Path: N:/3b2/HIPO/Vol00000/140122/APPFile/JW-HIPO140122

J_ID: za4 Customer A_ID: HIPO22361 Cadmus Art: HIPO22361 Ed. Ref. No.: 13-341.R2 Date: 16-September-14 Stage: Page: 15

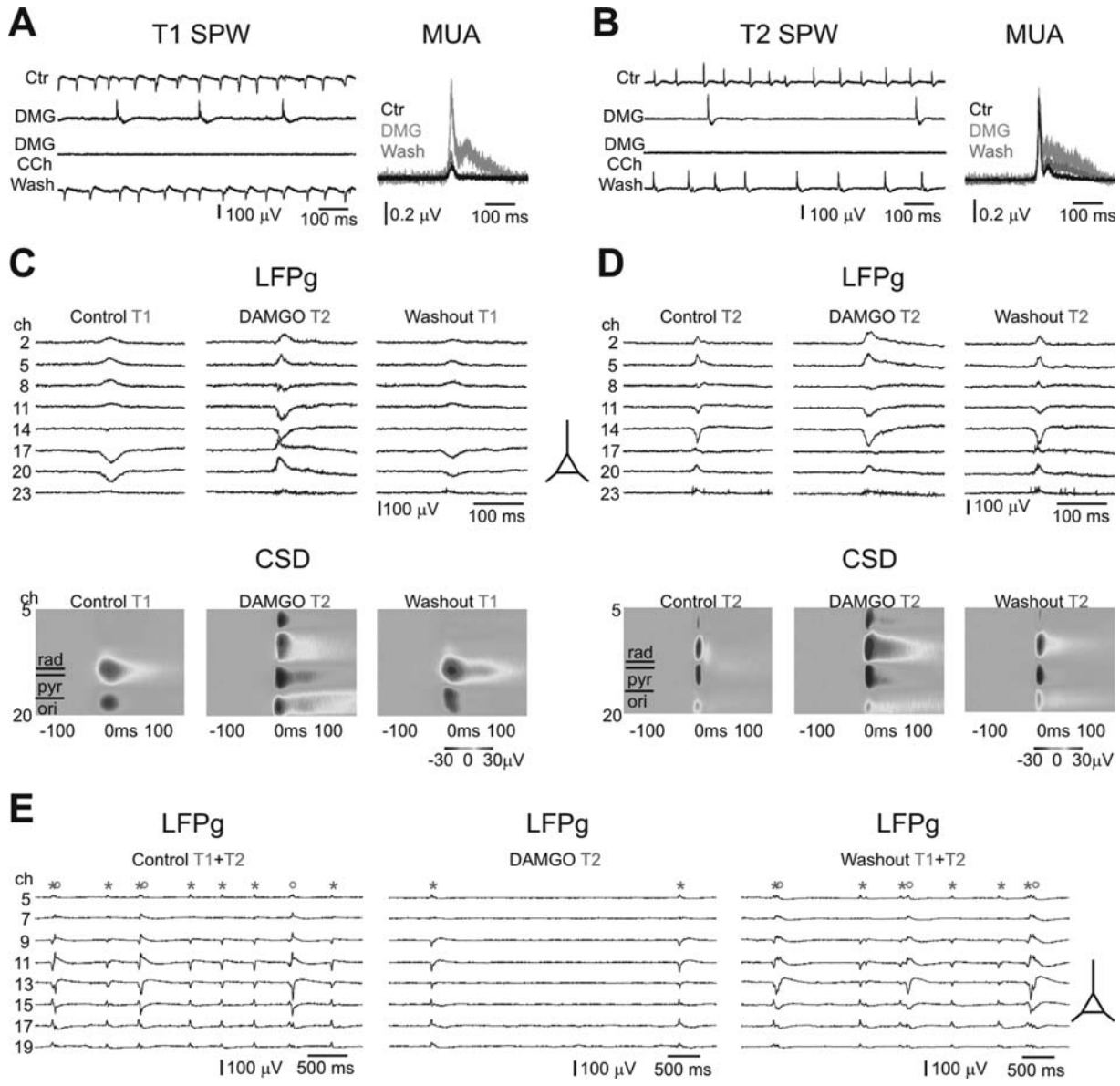

FIGURE 6. The application of the mu opioid recptor agonist DAMGO (DMG) significantly ($P < 0.001$) reduced the recurrence frequency of both T1 (A, left panel) and T2 (B, left panel) SPW-Rs. Further application of the cholinergic agonist carbachol (CCh) blocked the remaining SPW-R activity. The MUA was reversibly increased during DAMGO application for both T1 (A, right panel) and T2 (B, right panel) SPW-Rs (both significantly different, $P < 0.05$). The LFPg and CSD patterns of T1 SPW-Rs were converted into T2 SPW-Rs (C), while it remained unchanged for T2 SPW-Rs (D). Only T2 SPW-Rs could be detected during DAMGO application in slices with originally T1+T2 SPW-Rs (E). Schematic pyramidal cell shows the location of the cell layer and the orientation of the pyramidal cells. [Color figure can be viewed in the online issue, which is available at wileyonlinelibrary.com.]

was blocked ($n = 2$ cells), was desynchronized ($n = 4$ cells) or synchronized ($n = 5$ cells) in a bathing medium containing DAMGO. The changes in the firing rate and the firing pattern were not in correlation, thus further increased the heterogeneity of interneuronal behavior during DAMGO application (Supporting Information Tables 3 and 4, Supporting Information Fig. 6).

To diminish the activity of CB1-positive basket cells (Katona et al., 1999; Szabó et al., 2010), we further applied the acetylcholine receptor agonist CCh (5 μM) on slices where DAMGO reduced, but did not totally suppress SPW-R activity (Figs. 6A,B). In 8/8 slices with originally T1 SPW-Rs, in 4/5 with T2 SPW-Rs, and in 2/2 with T1+T2 SPW-Rs further application of CCh (in the presence of DAMGO) blocked the remaining SPW-Rs, and induced a slight gamma activity in 11/15 slices.

In summary, reducing the activity of parvalbumin-positive basket and somatostatin-positive dendritic inhibitory interneurons largely reduced the occurrence of both types of SPW-Rs, and reversibly converted T1 into T2 SPW-R. The remaining T2 SPW-Rs were blocked by cholinergic receptor activation.

ID: parasuramank Time: 14:12 I Path: N:/3b2/HIPO/Vol00000/140122/APPFile/JW-HIPO140122

J_ID: za4 Customer A_ID: HIPO22361 Cadmus Art: HIPO22361 Ed. Ref. No.: 13-341.R2 Date: 16-September-14 Stage: Page: 16

DISCUSSION

Generation of Synchronous Population Bursts

Rodent slice preparations exhibiting in vitro correlates of SPW-Rs provide an excellent tool to examine cellular and network properties of this population activity (Kubota et al., 2003; Maier et al., 2003; Colgin et al., 2004a; Behrens et al., 2005; Nimmrich et al., 2005; Wu et al., 2005a; Foffani et al., 2007; Ellender et al., 2010). Here, we report that the rat DG, CA3, and CA1 regions can generate spontaneous SPW-Rs in vitro in hippocampal slices. Two different types of SPW-Rs were observed in the CA3 region. Most CA3 pyramidal cells were hyperpolarized during both types of SPW-Rs. In accordance with the CSD source detected in the pyramidal cell layer, most recorded interneurons increased their firing rate, typically discharging before the LFPg peak of the SPW-Rs. Suppressing the activity of different subgroups of perisomatic inhibitory cells blocked the emergence of SPW-Rs.

Isolating regions from their afferent and efferent connections is a well established method to examine generators of population events involving multiple brain regions. Experiments using hippocampal slices without intrahippocampal connections provided different results. In several models including ours (Colgin et al., 2004a; Wu et al., 2005a; Foffani et al., 2007; Ellender et al., 2010), SPW-Rs could not be detected in the isolated CA1 region. In contrast, SPW-Rs could be detected in the isolated CA1 region in one model (Maier et al., 2003; Nimmrich et al., 2005). Similarly, synchronous population activity could be recorded [present study, (Maier et al., 2003; Colgin et al., 2004a,b)] or not (Wu et al., 2005a) in the isolated DG. All groups agreed that the isolated CA3 region generated SPW-Rs, suggesting that this region may play a key role in the initiation of these synchronous events.

Different SPW-R Patterns Are Generated by the Same Neuronal Network

Our data point to the existence of two different types of SPW-Rs in the CA3 region of rat hippocampal slices (Figs. 1 and 2). Type 1 SPW-Rs displayed negative LFPg peaks, while Type 2 SPW-Rs showed positive LFPg peaks in the pyramidal cell layer. Recurrence frequencies and CSD patterns were also different. This has not been reported in previous studies. One reason that we could separate them may be simply technical. The 24 channel laminar microelectrode, with contacts spaced at 50 μm, permitted excellent spatial sampling and facilitated CSD analysis. It clearly provides more detailed spatial data than recordings from 1 to 2 electrodes in the CA3 pyramidal cell layer (Kubota et al., 2003; Maier et al., 2003; Behrens et al., 2005; Nimmrich et al., 2005; Wu et al., 2006), although different SPW-R waveforms could be classified with the aid of a complex mathematical transformation (Reichinnek et al., 2010). Our data clearly demonstrate that the two types of SPW-Rs could be distinguished in LFPg recordings made with the laminar microelectrode, while the separation of the same SPW-Rs was not possible in records obtained with a one channel referential recording system (Fig. 2E, Supporting Information Fig. 7). Current source density analysis of SPW-Rs in vitro with a laminar multielectrode has been performed recently in the CA3 region of mouse hippocampal slices, where one type of SPW-R was detected (Hájos et al., 2013). This suggests that differences in the slice model might also account for the reason that multiple SPW-Rs have not been detected previously. The use of rat or mouse slices, age of the animal, dorsal or ventral hippocampus, horizontal, transverse or coronal slices, slice thickness, the use of interface, classical or dual perfusion (Hájos et al., 2009) submerged chamber, temperature and ionic composition of the bathing solution could all contribute to differences in the results. Altogether, our findings show clearly that the CA3 neuronal network can generate two distinct patterns of SPW-R activity (sometimes in the same slice, Fig. 2) in the rat hippocampus, in vitro.

Role of Excitatory Signaling

Excitatory circuits clearly participate in SPW-R generation in vitro. As in other studies (Maier et al., 2003; Colgin et al., 2004a; Behrens et al., 2005; Wu et al., 2005b; Ellender et al., 2010), SPW-Rs were reversibly abolished by blocking AMPA and KA type glutamate receptors (Fig. 3A). Multiple unit activity increased in records from the CA3 str. pyramidale during both types of SPW-Rs suggesting that pyramidal cell firing increased (Fig. 1), even though interneurons of this layer could also contribute. Our MUA data suggest more neuronal discharge during T1 than during T2 SPW-Rs (Figs. 1 and 2). In support of this view, higher ratios of cells showed depolarizing and biphasic responses (33.3% and 25.0%), and discharged (23.8% and 16.7%) during T1 than T2 SPW-Rs, respectively. Depolarizing components in responses of biphasic cells were also more frequent during T1 than during T2 SPW-Rs (78% and 11%, respectively), further strengthening the hypothesis that the activity of excitatory circuits is more pronounced during T1 than T2 SPW-Rs.

Depolarizing synaptic potentials were recorded from pyramidal cells that exhibited biphasic and depolarizing events during SPW-Rs (Fig. 4). At resting potential, 9 of these 11 cells also fired during SPW-Rs. In vivo, the CA3 region was proposed to be the generator region of SPW-Rs which are suggested to be triggered by a small subset of CA3 pyramidal cells acting as initiator cells (Buzsáki, 1989; Csicsvári et al., 2000). The group of pyramidal cells showing depolarizing and biphasic response may correspond to this subset of initiator cells.

Electrical stimulation of mossy fibers triggered comparable but slightly different transmembrane currents as the CSD pattern of spontaneous T1 SPW-Rs. This might suggest that T1 SPW-Rs are initiated in the dentate gyrus and are propagated to the CA3 region through mossy fibers. In contrast to this, our experiments showed that the activation of dentate granule cells is not required for the generation of T1 SPW-Rs: blocking mossy fiber activity or cutting the connection between the dentate gyrus and the CA3 region did not suppress T1 SPW-R

ID: parasuramank Time: 14:12 I Path: N:/3b2/HIPO/Vol00000/140122/APPFile/JW-HIPO140122

J_ID: za4 Customer A_ID: HIPO22361 Cadmus Art: HIPO22361 Ed. Ref. No.: 13-341.R2 Date: 16-September-14 Stage: Page: 17

activity (Fig. 3). Altogether, elimination of mossy fiber activity had only a slight impact on the emergence of both T1 and T2 SPW-Rs. These result are in contrast to a previous study (Rex et al., 2009) emphasizing the importance of mossy fibers in the generation of CA3 SPW-Rs. The differences in their model (slice thickness, angle of the ventral hippocampal slices, composition of the ACSF, higher concentration of mossy fiber blocker) might account for these opposing results.

Inhibitory Circuits Are Important for the Generation of SPW-Rs

Several of our experiments indicate the importance of inhibition in SPW-R generation. As previously reported (Maier et al., 2003; Behrens et al., 2005; Wu et al., 2005b; Ellender et al., 2010), SPW-Rs were reversibly blocked by GABAa receptor antagonists (Fig. 3B). We detected three different behaviors of CA3 pyramidal cells during SPW-Rs (Behrens et al., 2005; Wu et al., 2006; Ellender et al., 2010). Most cells were inhibited ($n = 32/43$), while only 7/43 showed a biphasic response consisting of a hyperpolarization with a superimposed excitatory potential, and 4/43 cells were excited during SPW-Rs. Most inhibitory interneurons ($n = 64/71$) showed a large increase in firing during SPW-Rs. Three quarters of recorded interneurons ($n = 53/71$ cells) discharged earlier than the peak of the SPW-R, thus they may participate in SPW-R initiation (Fig. 5). The high proportion of hyperpolarized pyramidal cells is consistent with the CSD source detected in the pyramidal cell layer. This source may reflect an active inhibitory current, implicating firing in perisomatic inhibitory cells. Indeed, suppressing the activity of certain perisomatic inhibitory cells largely decreased or even blocked the emergence of SPW-Rs (Fig. 6), confirming the hypothesis that perisomatic interneurons have an important role in SPW-R generation (Ellender et al., 2010; Hájos et al., 2013).

Our results support previous findings that distinct interneuron populations may be differentially involved (Hájos et al., 2013) in the generation of the two types of SPW-Rs. Interneurons with all different types of firing behavior were found to participate in the generation of T2 SPW-Rs, while only "SPW" and "SPW+blocked" interneurons seem likely to have contributed to T1 SPW-Rs (Fig. 5, Table 5). Additionally, we observed a layer-specificity in the firing pattern of interneuron populations: cells with "SPW+blocked" behavior were only present in the str. oriens. Nearly 60% of the interneurons ($n = 10/17$) recorded from slices exhibiting T1+T2 SPW-R activity behaved differently during the two types of SPW-Rs. Three of these cells enhanced their discharge rate during both types of SPW-Rs, but with a different firing behavior and different timing, whereas the large majority ($n = 7/10$) of the cells showed a highly related firing increase to one type, and no relation to the other type of SPW-R. A further interesting observation supports the differential contribution of distinct interneuron groups in the generation of SPW-R activities. Type 1 SPW-Rs were dynamically converted into T2 SPW-Rs by applying the mu opioid receptor agonist DAMGO (Fig. 6), indicating the relevance of parvalbumin-positive basket cells and somatostatin-positive dendritic inhibitory cells for the emergence of T1 SPW-Rs. The "SPW+blocked" firing pattern points to the possibility that interneuron-specific inhibitory cells are also activated during SPW-Rs, and reduce the firing rate of these cells following SPW-R events. In summary, the activation of distinct subsets of hippocampal interneurons is a key element in the reactivation of different ensembles of pyramidal cells, which finally results in the emergence of distinct SPW-R events.

CONCLUSIONS

One especially interesting insight emerging from this work is that the same hippocampal neuronal network can simultaneously generate multiple population activities. Different neuronal populations, with different proportions of pyramidal cells and distinct types of interneurons are activated during T1 and T2 SPW-Rs. The same pyramidal cell or interneuron can apparently participate in a different manner in these two activities. Activation of specific subpopulations of inhibitory cells—with the possible leading role of perisomatic interneurons—seems to be essential in the synchronization of distinct neuronal ensembles of CA3 pyramidal cells finally resulting in the expression of different SPW-R activities. This suggests that the hippocampus can generate dynamic changes in its activity stemming from the same excitatory and inhibitory circuits, and thus, might provide the cellular and network basis for input-specific information propagation.

Acknowledgments

The authors wish to thank Richárd Csercsa and Andor Magony for the data analysis program SpikeSolution and WaveSolution. Thanks to Dr. Richard Miles for useful comments on the manuscript.

REFERENCES

Bahner F, Weiss EK, Birke G, Maier N, Schmitz D, Rudolph U, Frotscher M, Traub RD, Both M, Draguhn A. 2011. Cellular correlate of assembly formation in oscillating hippocampal networks in vitro. Proc Natl Acad Sci USA 108:E607–E616.

Behrens CJ, van den Boom LP, de Hoz L, Friedman A, Heinemann U. 2005. Induction of sharp wave-ripple complexes in vitro and reorganization of hippocampal networks. Nat Neurosci 8:1560–1567.

Buzsáki G. 1986. Hippocampal sharp waves: Their origin and significance. Brain Res 398:242–252.

Buzsáki G. 1989. Two-stage model of memory trace formation: A role for 'noisy' brain states. Neuroscience 31:551–570.

Buzsáki G, Leung LW, Vanderwolf CH. 1983. Cellular bases of hippocampal EEG in the behaving rat. Brain Res 287:139–171.

ID: parasuramank Time: 14:12 I Path: N:/3b2/HIPO/Vol00000/140122/APPFile/JW-HIPO140122

J_ID: za4 Customer A_ID: HIPO22361 Cadmus Art: HIPO22361 Ed. Ref. No.: 13-341.R2 Date: 16-September-14 Stage: Page: 18

Buzsáki G, Horvath Z, Urioste R, Hetke J, Wise K. 1992. High-frequency network oscillation in the hippocampus. Science 256: 1025–1027.

Cohen I, Miles R. 2000. Contributions of intrinsic and synaptic activities to the generation of neuronal discharges in in vitro hippocampus. J Physiol 524 Part 2:485–502.

Colgin LL, Jia Y, Sabatier JM, Lynch G. 2005. Blockade of NMDA receptors enhances spontaneous sharp waves in rat hippocampal slices. Neurosci Lett 385:46–51.

Colgin LL, Kubota D, Jia Y, Rex CS, Lynch G. 2004a. Long-term potentiation is impaired in rat hippocampal slices that produce spontaneous sharp waves. J Physiol 558:953–961.

Colgin LL, Kubota D, Brucher FA, Jia Y, Branyan E, Gall CM, Lynch G. 2004b. Spontaneous waves in the dentate gyrus of slices from the ventral hippocampus. J Neurophysiol 92:3385–3398.

Csicsvári J, Hirase H, Mamiya A, Buzsáki G. 2000. Ensemble patterns of hippocampal CA3-CA1 neurons during sharp wave-associated population events. Neuron 28:585–594.

Csicsvári J, Hirase H, Czurko A, Mamiya A, Buzsáki G. 1999. Oscillatory coupling of hippocampal pyramidal cells and interneurons in the behaving Rat. J Neurosci 19:274–287.

Drake CT, Milner TA. 2002. Mu opioid receptors are in discrete hippocampal interneuron subpopulations. Hippocampus 12:119–136.

Ellender TJ, Nissen W, Colgin LL, Mann EO, Paulsen O. 2010. Priming of hippocampal population bursts by individual perisomatic-targeting interneurons. J Neurosci 30:5979–5991.

Fabó D, Maglóczky Z, Wittner L, Pék A, Erőss L, Czirják S, Vajda J, Sólyom A, Rásonyi G, Szucs A, Kelemen A, Juhos V, Grand L, Dombovári B, Halász P, Freund TF, Halgren E, Karmos G, Ulbert I. 2008. Properties of in vivo interictal spike generation in the human subiculum. Brain 131:485–499.

Foffani G, Uzcategui YG, Gal B, Menendez de la Prida L. 2007. Reduced spike-timing reliability correlates with the emergence of fast ripples in the rat epileptic hippocampus. Neuron 55:930–941.

Freeman JA, Nicholson C. 1975. Experimental optimization of current source-density technique for anuran cerebellum. J Neurophysiol 38:369–382.

Freund TF, Buzsáki G. 1996. Interneurons of the hippocampus. Hippocampus 6:347–470.

Freund TF, Katona I. 2007. Perisomatic inhibition. Neuron 56:33–42.

Giannopoulos P, Papatheodoropoulos C. 2013. Effects of mu-opioid receptor modulation on the hippocampal network activity of sharp wave and ripples. Br J Pharmacol 168:1146–1164.

Gulyás AI, Szabó GG, Ulbert I, Holderith N, Monyer H, Erdélyi F, Szabó G, Freund TF, Hájos N. 2010. Parvalbumin-containing fast-spiking basket cells generate the field potential oscillations induced by cholinergic receptor activation in the hippocampus. J Neurosci 30:15134–15145.

Hájos N, Ellender TJ, Zemankovics R, Mann EO, Exley R, Cragg SJ, Freund TF, Paulsen O. 2009. Maintaining network activity in submerged hippocampal slices: Importance of oxygen supply. Eur J Neurosci 29:319–327.

Hájos N, Karlócai MR, Németh B, Ulbert I, Monyer H, Szabó G, Erdélyi F, Freund TF, Gulyás AI. 2013. Input-output features of anatomically identified CA3 neurons during hippocampal sharp wave/ripple oscillation in vitro. J Neurosci 33:11677–11691.

Hazan L, Zugaro M, Buzsáki G. 2006. Klusters, NeuroScope, NDManager: A free software suite for neurophysiological data processing and visualization. J Neurosci Methods 155:207–216.

Kamiya H, Shinozaki H, Yamamoto C. 1996. Activation of metabotropic glutamate receptor type 2/3 suppresses transmission at rat hippocampal mossy fibre synapses. J Physiol 493 (Part 2):447–455.

Kano T, Inaba Y, Avoli M. 2005. Periodic oscillatory activity in parahippocampal slices maintained in vitro. Neuroscience 130:1041–1053.

Katona I, Sperlágh B, Sík A, Kafalvi A, Vizi ES, Mackie K, Freund TF. 1999. Presynaptically located CB1 cannabinoid receptors regulate GABA release from axon terminals of specific hippocampal interneurons. J Neurosci 19:4544–4558.

Kubota D, Colgin LL, Casale M, Brucher FA, Lynch G. 2003. Endogenous waves in hippocampal slices. J Neurophysiol 89:81–89.

Maier N, Nimmrich V, Draguhn A. 2003. Cellular and network mechanisms underlying spontaneous sharp wave-ripple complexes in mouse hippocampal slices. J Physiol 550:873–887.

Miles R, Tóth K, Gulyás AI, Hájos N, Freund TF. 1996. Differences between somatic and dendritic inhibition in the hippocampus. Neuron 16:815–823.

Nicholson C, Freeman JA. 1975. Theory of current source-density analysis and determination of conductivity tensor for anuran cerebellum. J Neurophysiol 38:356–368.

Nimmrich V, Maier N, Schmitz D, Draguhn A. 2005. Induced sharp wave-ripple complexes in the absence of synaptic inhibition in mouse hippocampal slices. J Physiol 563:663–670.

Papatheodoropoulos C. 2008. A possible role of ectopic action potentials in the in vitro hippocampal sharp wave-ripple complexes. Neuroscience 157:495–501.

Papatheodoropoulos C, Kostopoulos G. 2002a. Spontaneous, low frequency (approximately 2–3 Hz) field activity generated in rat ventral hippocampal slices perfused with normal medium. Brain Res Bull 57:187–193.

Papatheodoropoulos C, Kostopoulos G. 2002b. Spontaneous GABA(A)-dependent synchronous periodic activity in adult rat ventral hippocampal slices. Neurosci Lett 319:17–20.

Paxinos G, Watson C. 1998. The Rat Brain in Stereotaxic Coordinates, 4th ed. San Diego, CA: Academic Press.

Reichinnek S, Kunsting T, Draguhn A, Both M. 2010. Field potential signature of distinct multicellular activity patterns in the mouse hippocampus. J Neurosci 30:15441–15449.

Rex CS, Colgin LL, Jia Y, Casale M, Yanagihara TK, Debenedetti M, Gall CM, Kramar EA, Lynch G. 2009. Origins of an intrinsic hippocampal EEG pattern. PLoS One 4:e7761.

Szabó GG, Holderith N, Gulyás AI, Freund TF, Hájos N. 2010. Distinct synaptic properties of perisomatic inhibitory cell types and their different modulation by cholinergic receptor activation in the CA3 region of the mouse hippocampus. Eur J Neurosci 31:2234–2246.

Ulbert I, Halgren E, Heit G, Karmos G. 2001. Multiple microelectrode-recording system for human intracortical applications. J Neurosci Methods 106:69–79.

Ulbert I, Heit G, Madsen J, Karmos G, Halgren E. 2004a. Laminar analysis of human neocortical interictal spike generation and propagation: Current source density and multiunit analysis in vivo. Epilepsia 45 (Suppl 4):48–56.

Ulbert I, Maglóczky Z, Erőss L, Czirják S, Vajda J, Bognár L, Tóth S, Szabó Z, Halász P, Fabó D, Halgren E, Freund TF, Karmos G. 2004b. In vivo laminar electrophysiology co-registered with histology in the hippocampus of patients with temporal lobe epilepsy. Exp Neurol 187:310–318.

Wu C, Asl MN, Gillis J, Skinner FK, Zhang L. 2005a. An in vitro model of hippocampal sharp waves: regional initiation and intracellular correlates. J Neurophysiol 94:741–753.

Wu C, Luk WP, Gillis J, Skinner F, Zhang L. 2005b. Size does matter: Generation of intrinsic network rhythms in thick mouse hippocampal slices. J Neurophysiol 93:2302–2317.

Wu CP, Huang HL, Asl MN, He JW, Gillis J, Skinner FK, Zhang L. 2006. Spontaneous rhythmic field potentials of isolated mouse hippocampal-subicular-entorhinal cortices in vitro. J Physiol 576: 457–476.

Ylinen A, Bragin A, Nádasdy Z, Jandó G, Szabó I, Sík A, Buzsáki G. 1995. Sharp wave-associated high-frequency oscillation (200 Hz) in the intact hippocampus: Network and intracellular mechanisms. J Neurosci 15:30–46.

ID: parasuramank Time: 14:12 I Path: N:/3b2/HIPO/Vol00000/140122/APPFile/JW-HIPO140122

AQ1: Please confirm that all author names are OK and are set with first name first, surname last.

AQ2: Please confirm whether the color figures should be reproduced in color or black and white in the print version. If the color figures must be reproduced in color in the print version, please fill the color charge form immediately and return to Production Editor. Or else, the color figures for your article will appear in color in the online version only.

AQ3: Please provide the department and university names for affiliations 1 and 3.